ICARUS **126,** 261–281 (1997)
ARTICLE NO. IS965647

Protoplanet Migration by Nebula Tides

WILLIAM R. WARD[1]

Jet Propulsion Laboratory, California Institute of Technology, Pasadena, California 91109

Received November 27, 1995; revised October 7, 1996

The tidal interaction of a protoplanet with a circumstellar gaseous disk results in mutual angular momentum exchange that modifies both the disk and the orbit of the secondary. There are two, conceptually distinct circumstances wherein nebula torques can cause a secular variation in a protoplanet's semimajor axis. (I) The net torque exerted on a secondary by an undisturbed disk is not, in general, zero. Although gradients in the disk density and temperature can contribute to this torque, it is mostly due to asymmetries in the disk/planet interaction that are inherent to a Keplerian disk. For a relatively thick disk, the differential torque can be a significant fraction of the torque from either its exterior or its interior portion. In this case, the protoplanet drifts relative to disk material on a time scale inversely proportional to its mass. (II) The protoplanet opens a gap in the disk that establishes a flow barrier to disk material. A density discontinuity that locks the protoplanet into the disk's viscous evolution develops across the orbit. The protoplanet migrates on a time scale set by the disk's viscosity.

A unified model that clarifies the relationship between these migration types and reveals under what circumstances a given type is selected is presented. In both cases, orbital decay is the prevailing outcome, although type I migration rates can be between one and two orders of magnitudes faster than type II. Estimates of orbital lifetimes are given and are generally shorter than the expected lifetime of the disk. Some implications to the issue of planetary formation are discussed.

I. INTRODUCTION

The excess infrared radiation observed to be a common feature associated with young stars has led to the discovery of numerous circumstellar disks of gas and/or dust of the sort thought to be planetary progenitors (e.g., Walter *et al.* 1988, Beckwith and Sargent 1993). This constitutes strong circumstantial evidence that planetary systems could be quite numerous as well. Indeed, the surprising detection of companions orbiting Pulsar PSR B1257+12 (Wolszczan 1994) reveals that planets can exist in a variety of environments, including some that might once have been considered unlikely. On the other hand, the recently reported searches for Jupiter sized planets suggest that such objects may be less numerous than expected (Cochran and Hatzes 1993, Marcy and Butler 1992, McMillan *et al.* 1994, Walker *et al.* 1995; see also Black 1995). In over 200 candidate stars observed so far, the yield has been only ~3%. Furthermore, the recently discovered planet around 51 Pegasi (Mayor and Queloz 1995) occupies such a tight orbit (i.e., 0.05 AU), that it seems unlikely that this is its original state. Other newly discovered candidates around tau Bootis, upsilon Andromedea, and 55 rho Cancri also have suspiciously small semimajor axes for gas giants. Of course, the low yield may be strongly influenced by selection effects, since large planets close to their primaries are easier to detect. Even so, these results pose some natural questions: How likely is it that a given circumstellar disk will produce a planetary system? Is a combination of terrestrial and giant planets a typical or an unusual outcome? Once formed, are there forces that tend to destroy a system?

Current models of planetary formation tend to partition events into three broad stages (e.g., Wetherill 1990, Lissauer and Stewart 1993, Lissauer 1993, Ward 1995): (i) the fractionation of solids from the gaseous nebula, with the formation of planetesimals in a thin subdisk, (ii) the accumulation of $O(10^3)$ km-sized protoplanetary embryos by binary accretion, and (iii) the ultimate combination of these embryos into planetary bodies. In the case of the giant planets, this final stage also involves a substantial gas accretion phase as well. Although each of these broad stages involves multiple processes, and the boundaries between them are by no means sharply defined; they are, nevertheless, convenient starting points for theoretical studies of specific aspects of planet building.

An obviously important goal is to identify and include the most essential physical and chemical processes that characterize each stage of growth. To date, the most extensively modeled is the mid-stage, during which planetary embryos are believed to develop relatively quickly (i.e., $O(10^{5-6})$ years) through accretion runaway (e.g., Lissauer

[1] Also at San Juan Capistrano Research Institute, San Juan Capistrano, CA.

0019-1035/97 $25.00

and Stewart 1993, and references therein). In contrast, the late-stage mechanisms by which the final planets are assembled from these embryos are more problematic. Relying on gravitational relaxation of the disk to excite orbital eccentricities and produce crossing orbits seems to work well for our inner planets, where orbital periods are shorter (e.g., Wetherill 1990). However, this picture runs into difficulties when applied to the giant planets, which clearly must form within the lifetime of the gas disk. The observed prevalence of disks among young stars suggests that these structures have lifetimes of only 10^6–10^7 years (Walter *et al.* 1988), providing a tight constraint on the time available to accumulate a giant planet core of some 10–30 Earth masses.

The coexistence of the nebula and protoplanets presents an intriguing question: Could the presence of the gas phase have been a key component in the rapid accumulation of solid bodies? Of course, researchers have long acknowledged the possible importance of aerodynamic drag in the early-stage formation of planetesimals (e.g., Weidenschilling 1977; Hayashi *et al.* 1977). However, traditional drag effects are proportional to a body's cross section and, because of their diminishing surface to volume ratios, become relatively unimportant once objects exceed kilometers in radius. Consequently, gas probably has only a modest influence on mid-stage growth mechanisms. On the other hand, as we will argue in the next section, there is good reason to believe that for large enough objects, the gas disk may again become an important player. The strong gravitational coupling between protoplanetary bodies and their precursor disk may generate a surprising degree of radial mobility (Ward 1986, 1989, Lin and Paploizou 1993). This migration constitutes a double edged sword: it may at once assist in a protoplanet's accretion and place its ultimate survival in jeopardy.

II. DISK TIDES

A protoplanet can gravitationally interact with the disk at resonance sites (Lynden-Bell and Kalnajs 1972). At sites of *Lindblad* resonances, where the Doppler shifted forcing frequency matches the natural oscillation frequency of the disk, this disturbance takes the form of a spiral wave that, in a pressure dominated disk, propagates away from the resonance zone (e.g., Goldreich and Tremaine 1979). The protoplanet's gravitational attraction for this wave results in a reaction torque.

a. Drift Modes

Goldreich and Tremaine (1980; hereafter referred to as GT80) were the first to suggest that large objects could migrate as a result of these disk torques, referred to collectively as disk tides. This would constitute an unexploited degree of radial mobility that could have important consequences for late-stage accretion models (e.g., Hourigan and Ward 1984, Ward 1989, 1993a). Although the existence of this mechanism has been acknowledged in the literature, there has developed some confusion over the exact nature and rate of this orbital drift. There are actually two conceptually distinct circumstances wherein nebula torques could cause a secular variation in a protoplanet's semimajor axis.

(I) In general, the net torque exerted on a secondary by an undisturbed disk is *not* zero (Ward 1986, Korycansky and Pollack 1993, Artymowicz 1993). This is due to a mismatch in the positive interior and negative exterior disk torques exerted on the protoplanet. In this case, the net torque causes the protoplanet to drift *relative* to the disk material on a time scale that is inversely proportional to its mass and the mass of the disk. This is essentially the mechanism described by Goldreich and Tremaine.[2] Variations in the global properties of the disk can be expected to produce a fractional torque mismatch of a given mth order Lindblad pair. This leads to a differential torque $\Delta T \approx (c_1/2)\mu^2\sigma r^2(r\Omega)^2(r\Omega/c)^3$ and corresponding migration rate of order

$$v = c_1\mu(r\Omega)(\sigma r^2/M_\mathrm{p})(r\Omega/c)^3, \qquad (1)$$

where μ is the mass of the protoplanet normalized to the primary's mass, M_p, σ is the surface density of the disk, and c_1 is a measure of the torque asymmetry.[3] Dimensional arguments suggest that c_1 should scale with h/r (GT80) and $v \propto (r\Omega/c)^2$. We refer to this drift as type I.

(II) If the disk spreads under the influence of viscous shear stresses (Lynden-Bell and Pringle 1974), a second method of migration is for the protoplanet to establish a tidal barrier to the flow of gas across its orbit. This is generally accompanied by the formation of a gap that *locks* the planet into the angular momentum transport processes of the nebula. The interior portion of the disk still exerts a torque on the planet, which in turn exerts a torque on the exterior portion of the disk. Consequently, angular momentum can be transported across the orbit, even if gas cannot. A density discontinuity will build up on one side of the planet until a sufficient torque imbalance develops

[2] Ironically, although the pioneering work in GT80 laid the ground work for many subsequent studies, the paper itself contained an inconsistency in the reported rates for eccentricity and semimajor axis variations of their example application—that of a jovian sized perturber in a minimum mass solar nebula. Their semimajor axis drift rate is valid only in the absence of a gap, while the eccentricity decay rate is valid only if a gap exists (see Ward 1988). Generally speaking, larger planets should be more successful in opening a gap and it seems likely that a jovian sized object would do so, thereby drifting on the disk's viscous time scale instead of exhibiting the very rapid (i.e., $\sim O(10^4)$ years) orbit migration reported in GT80. Nevertheless, smaller (but still substantial) objects may well behave as suggested by Goldreich and Tremaine.

[3] Note that this definition of c_1 defers from the parameter C used in earlier works (e.g., Ward 1986) by a factor of order h/r.

to "push" the planet along with the disk material (e.g., Ward 1982, Lin and Papaloizou 1986b, 1993). Thereafter the system coevolves on the viscous time scale of the disk, with a radial velocity of order $v \sim O(\nu/r)$, where ν is the kinematic viscosity of the gas—believed to be primarily due to turbulence. Representing the viscosity by a Shakura–Sunyaev form, $\nu \sim \alpha c^2/\Omega$, the characteristic velocity for this type of migration is

$$v = c_2 \alpha (r\Omega)(c/r\Omega)^2, \tag{2}$$

where r and Ω are the orbital radius and angular frequency respectively, c is the gas sound speed, and c_2 is a constant on order unity. We shall refer to Eq. (2) as type II drift. Current estimates for α in the solar nebula lie in the range 10^{-4}–10^{-2} (e.g., Cabot *et al.* 1987, Dubrulle 1993), while the ratio of sound to orbital velocity is typically of order *few* $\times 10^{-2}$. Numerical models of this process have been presented by Lin and Papaloizou (1986b, 1993).

Whether or not the perturber is able to create a gap in the disk is thus a key issue in determining its mode of interaction. These two types of drift have not always been properly distinguished in the literature. In Section III, a unified model for quasi-steady-state drift of a protoplanet is presented in which these two drift types are found to be limiting cases of weak and strong coupling, respectively. However, we first address the issue of torque strength.

b. Torque Strength

The torque exerted on the disk in the vicinity of an mth order Lindblad resonance is (Appendix A),

$$T_m = -\frac{\pi^2 m \sigma \Psi_m^2}{r dD_*/dr}. \tag{3}$$

This is a generalized version of the expression given by Goldreich and Tremaine (1978, 1979). In Eq. (3), Ψ_m is the forcing function due to the secondary (Artymowicz, 1993a),[4]

$$\Psi_m = \frac{r d\phi_m/dr + 2mf\phi_m}{\sqrt{1 + 4\xi^2}}, \tag{4}$$

where ϕ_m is the amplitude of the disturbing function's mth order Fourier component, $\xi \equiv mc/r\kappa$, $f = m(\Omega - \Omega_s)/\Omega$, and

$$D_* \equiv D + (mc/r)^2, \tag{5}$$

[4] The form given by Artymowicz contains an additional factor $(1 + \xi^2)^{-1/4}$, which in our formulation has been incorporated into rdD_*/dr.

where $D \equiv \kappa^2 - m^2(\Omega - \Omega_s)^2$ is a measure of the difference between the local epicycle frequency of the disk, κ, and the Doppler shifted forcing frequency, $m|\Omega - \Omega_s|$. (The subscript s has been introduced to refer to the secondary.) The potential amplitude for $m > 1$ is

$$\phi_m = -\frac{GM_s}{r_s} b_{1/2}^m(\alpha_r), \tag{6}$$

where

$$b_{1/2}^m(\alpha_r) \equiv \frac{2}{\pi}\int_0^\pi \frac{\cos m\theta \, d\theta}{\sqrt{1 - 2\alpha_r \cos\theta + \alpha_r^2}} \tag{7}$$

is the Laplace coefficient with argument $\alpha_r \equiv r/r_s$. In writing Eq. (4), we have chosen a form that is valid when the driving potential varies little over the first cycle of the wave (Artymowicz, 1993a). This assumption is only marginally valid for the most important resonances, but greatly simplifies the analysis. Since our primary objective is to illustrate the mechanisms of protoplanet drift, we believe the essential nature of the process is not affected by this choice. The close agreement of the numerical results of Korycansky and Pollack (1993) with our derived differential torque lends support to this contention. The total disk torque is found by summing the contributions from all resonances, both inside and outside the protoplanet's orbit.

Earlier studies of protoplanet migration used a simplified torque expression in which torque asymmetry arose only from variations in the surface density (Hourigan and Ward 1984, Ward and Hourigan 1989, Lin and Papaloizou 1986, 1993). Ward (1986) improved on this by including other structural gradients in the calculation. Further developments in the theory of Lindblad resonance interaction, especially the behavior of the so-called torque cutoff phenomenon (Artymowicz 1993a,b), now make possible a much improved prescription for the torque. Much of this improvement is realized by evaluating all quantities in Eq. (3) where $D_* = 0$, which gives the location for an mth order Lindblad resonance, corrected for the effects of pressure on the natural oscillation frequency of the disk (Ward 1988, Artymowicz 1993a). After some manipulation (Appendix A), this leads to the torque expression

$$T_m = \varepsilon \frac{4}{3}\mu^2(\sigma r_s^2)(r_s\Omega_s)^2 \frac{m^2\alpha^{3/2}\psi^2}{q\sqrt{1 + \xi^2}(1 + 4\xi^2)}, \tag{8}$$

where

$$\psi = \frac{\pi}{2}\left[\frac{1}{m}\left|\frac{db_{1/2}^m(\alpha_r)}{d\alpha_r}\right| + 2\sqrt{1 + \xi^2}\, b_{1/2}^m(\alpha_r)\right] \tag{9}$$

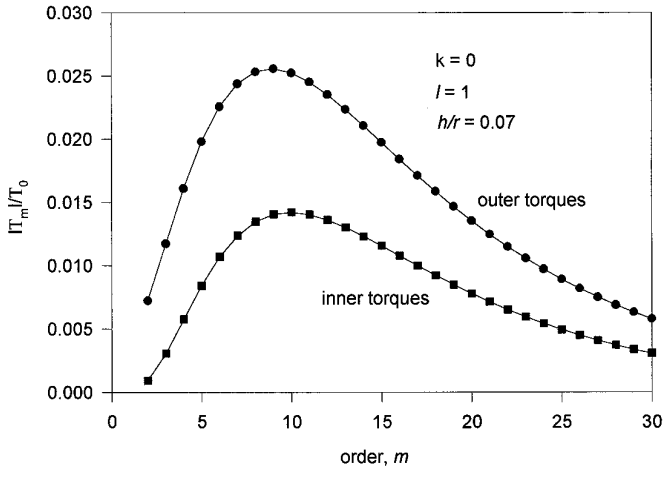

FIG. 1. Torque magnitude as a function of order, m, normalized to the reference value, $T_o = \mu^2\mu_g M_p(r_s\Omega_s)^2/h_s'^3$, for a disk of constant density and normalized scale height, $h' = 0.07$. Maximum values occur for $m \sim 8$–9; decrease of torque at higher order is due to torque cutoff phenomenon.

$q(\xi) \equiv 1 - \varepsilon(1 - l)h'/3\alpha^{3/2} \cdot \xi/\sqrt{1 + \xi^2}$ being a weak function of ξ, and where we have set $\kappa \approx \Omega$. In these expressions, $\varepsilon = 1$ (-1) for outer (inner) resonances. The orbital frequency of the disk is taken to be

$$\Omega^2 = \Omega_K^2 - (k + l)\frac{c^2}{r^2}, \tag{10}$$

where $\Omega_K^2 \equiv GM_p/r^3$, is the Keplerian rate. The second term corrects for the radial support of the pressure gradient due to density gradient, $k \equiv -d \ln \sigma/d \ln r$, and temperature gradient, $l \equiv -d \ln T/d \ln r$.

Equation (8) is plotted in Fig. 1 for a disk with constant surface density ($k = 0$) and constant normalized scale height ($l = 1$), set to $h/r = 0.07$. The torques $|\hat{T}_m| \equiv |T_m|/T_o$ are normalized to a reference value, $T_o \equiv \mu^2\mu_g M_p(r_s\Omega_s)^2(r_s/h_s)^3$, where $\mu_g \equiv \pi\sigma_s r_s^2/M_p$ is the nondimensional disk mass.[5] The "intrinsic" torque asymmetry predicted by Ward (1986) and confirmed numerically by Korycansky and Pollack (1993) is apparent. There are three sources of asymmetry in the interaction of the secondary with a Keplerian disk[6]:

(1) The gradient of the frequency separation, rdD_*/dr, in the denominator of Eq. (3) is proportional to the epicycle frequency, κ, which is always smaller for outer resonances.

(2) Outer resonances lie slightly closer to the perturber than inner resonances of the same order and thereby sample the monotonically decreasing forcing function at a greater value.

(3) Even if the resonances were symmetrically positioned, the forcing function, Ψ_m, is systematically larger near an outer resonance than in the vicinity of a complimentary inner one. This is due in large part to the appearance of f in the numerator of its definition, Eq. (4).

All three of these traits conspire to make the outer disk torque stronger, and their relative importance is traced in Appendix B. *The resulting negative net torque implies that the prevailing radial drift is one of orbital decay.*

Recall that in the example of Fig. 1, the torque differential for a given order, m, does *not* come from a density contrast between the outer and inner Lindblad resonance sites. In fact, a global density gradient in the disk turns out to be less important than originally thought because of a "buffering" action between the density gradient and its associated pressure gradient, these two tending to work in opposition (Ward 1986, Korycansky and Pollack 1993). While a larger k enhances the density contrast, by that increasing the relative strength of the inner torques over the outer, the associated pressure gradient alters the rotational profile of the disk [i.e., Eq. (10)] shifting the resonance positions inward, thereby increasing the strength of the outer resonances compared with the inner. As an example, Fig. 2a shows the torques for a disk with $k = 3/2$, $l = \frac{1}{2}$ without resonance shifts, while Fig. 2b shows the torques with the pressure buffer included. In Fig. 3a, the net normalized torque, $\Gamma_1 \equiv \sum \hat{T}_m$, is plotted as a function of k with (closed symbols) and without (open symbols) the buffer. The pressure buffer renders the net torque insensitive to k. On the other hand, the torque asymmetry *is* sensitive to the gradient in the disk temperature, since this too can shift resonance positions. Here, a larger l increases the net negative torque as shown in Fig. 3b.

c. Torque Density

If the distance between resonance sites is less than the driving distance for the waves, a smoothed torque density, $dT/dr = T_m|dm/dr|$, can be defined (e.g., GT80, Meyer-Vernet and Sicardy 1987). From Eq. (5) we find

$$\frac{dm}{dr} = -\frac{\partial D_*/\partial r}{\partial D_*/\partial m} = \frac{m}{2\kappa^2}\frac{dD_*}{dr}, \tag{11}$$

while the driving distance for pressure waves is of order (e.g., Ward 1986, Artymowicz 1993)

$$\lambda_{\text{driving}} \approx \left(\frac{c^2}{dD_*/dr}\right)^{1/3}. \tag{12}$$

[5] Strictly speaking, μ_g would be the normalized mass interior to the protoplanet for a constant density disk, but is commonly referred to by the shorthand "disk mass."

[6] These asymmetries did not appear in the original formulation of GT80 because the authors set $\alpha_r = 1$, unless it appeared in the combination, $\alpha_r - 1$, which was then set equal to $\pm 2/3m$ as the resonant values.

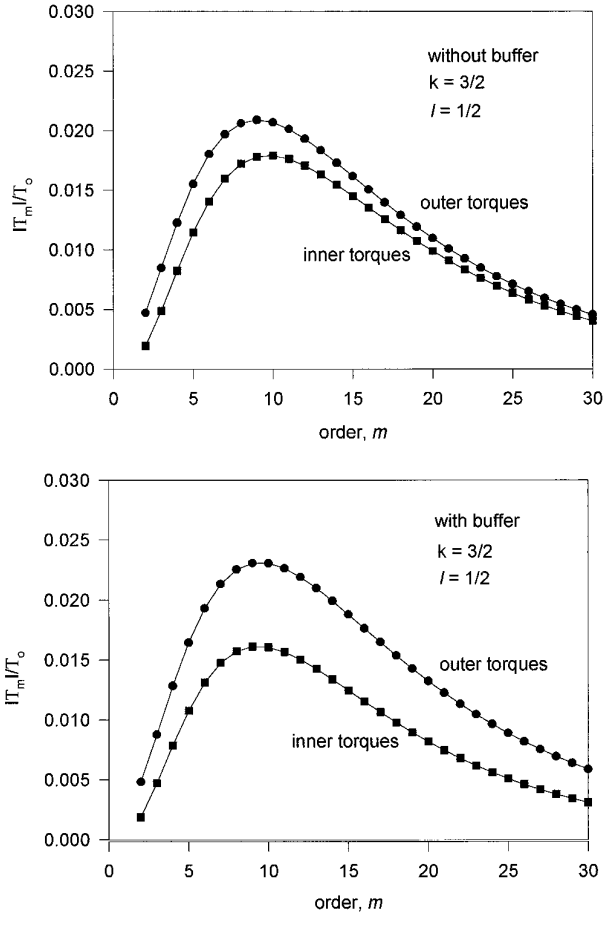

FIG. 2. Torque magnitudes as a function of order for a disk with surface density $\sigma \propto r^{-3/2}$, when (a) resonance positions are not adjusted due to pressure gradient modification of disk rotation and (b) shifts in the resonance positions are taken into account (pressure buffer).

The driving distance is greater than $|dm/dr|^{-1}$ for $m \geq h'^{-2/5} \approx 2.5$. The smoothed torque density is

$$\frac{dT}{dr} \equiv T_m \left| \frac{dm}{dr} \right| = \varepsilon \frac{\pi^2 m^2 \sigma \Psi^2}{2r\kappa^2}. \tag{13}$$

Combining with Eqs. (4) and (9) yields

$$\frac{dT}{dr} = \varepsilon \frac{2\mu^2(\sigma r_s^2)(r_s\Omega_s)^2 m^4 \psi^2}{r(1+4\xi^2)} \left(\frac{\Omega_S}{\kappa}\right)^2. \tag{14}$$

Here m is treated as a continuous function of r given by

$$m(r) = \sqrt{\frac{\kappa^2}{(\Omega - \Omega_s)^2 - c^2/r^2}}. \tag{15}$$

The quantity, $d\hat{T}/dx = (h_s/T_o)\, dT/dr$ is plotted in Fig. 4. Notice that the torque density is zero in an annulus surrounding the perturber. This is because no real solutions for Eq. (15) exist when $|\Omega - \Omega_s| < c/r$, so that Lindblad resonances are excluded from the region $\pm O(2h/3)$. In the true torque density, which is given by the superposition of the spatial driving of all waves, the falloff would be less precipitous because *some* driving of the wave occurs inside the nominal resonance position, $D_* = 0$. Even so, the maximum torque is due to the disk material at radial distances comparable to the scale height, with little torque exerted by disk material inside this region.

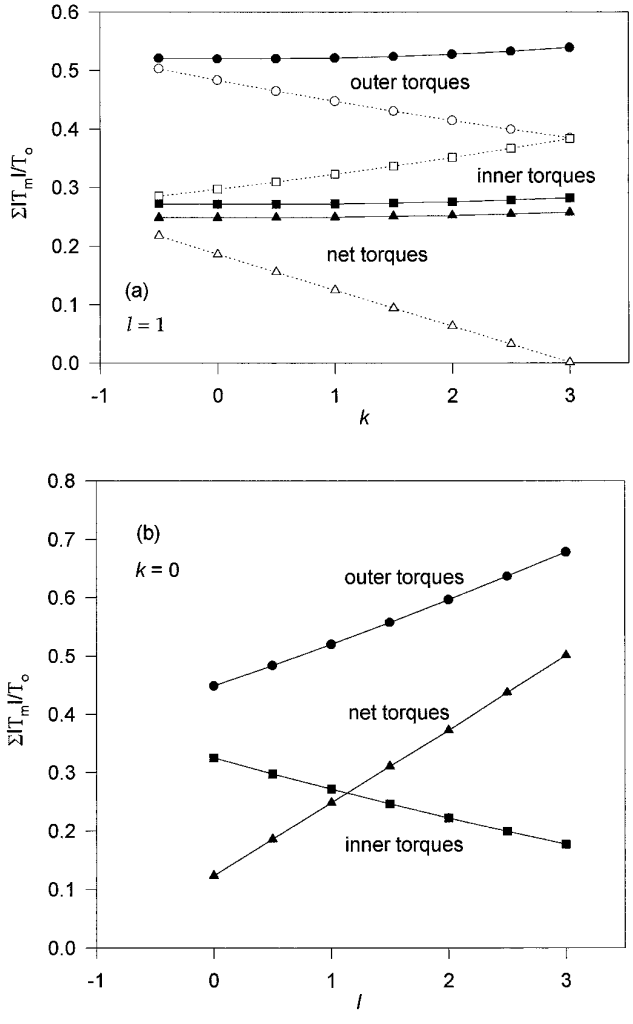

FIG. 3. Total inner and outer torque summed over order and their difference (net torque). (a) Torques as a function of $k \equiv -(r/\sigma)\, d\sigma/dr$ for a disk of constant h' without pressure buffer correction (open symbols) and with buffer included (filled symbols). (b) Torque as a function of $l \equiv -(r/T)\, dT/dr$ for a disk of constant surface density.

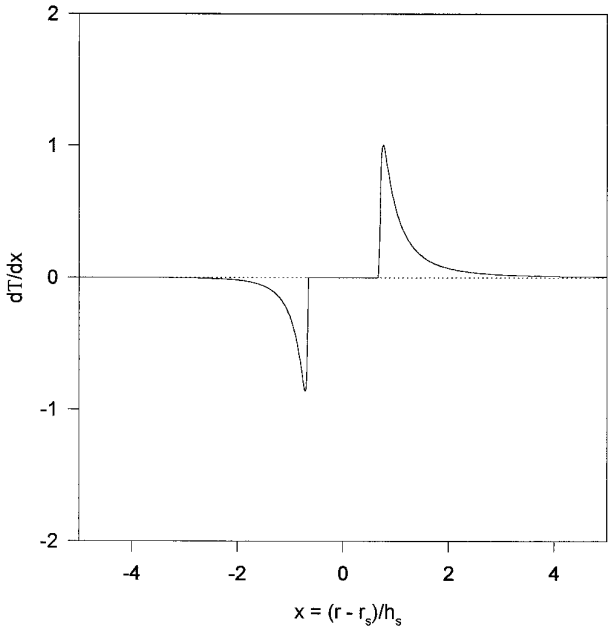

FIG. 4. Normalized torque density, $\hat{T}_m|dm/dx|$, as a function of distance from perturber in units of the disk scale height. Region of zero torque surrounding perturber with half width $2h/3$ is torque cutoff zone.

d. Local Damping Limit

In much of this paper we make the important simplifying assumption that the deposition of angular momentum in the disk has the same spatial distribution as the torque density; i.e., $dT/dr|_{\rm disk} = dT/dr$. This is not necessarily the case, since wave action transports angular momentum until the waves are damped. Thus, this procedure is tantamount to assuming that waves damp locally. Our motivation is to first work the case most conducive to gap formation in order to establish the minimum mass range for type I behavior. However, local damping is not without some justification. Recent work by Cassen and Woolum (1996) shows that radiation damping can dissipate waves over a distance $\delta_{\rm rad} \sim \sigma c^3/2\sigma_{\rm SB}T^4 f_{\rm D}$, where $\sigma_{\rm SB}$ is the Stefan–Boltzman constant and $f_{\rm D}$ is a weak decreasing function of the optical depth that varies from order unity to $\sim$0.1 as the optical depth increases from unity to $\sim 10^5$. The damping to driving length ratio is $\delta_{\rm rad}/\lambda_{\rm driving} \approx 0.5m^{1/3}\sigma_2/f_{\rm D}T_2^{17/6}$, where $\{\sigma_2, T_2\} \equiv \{\sigma, T\} \times 10^{-2}$. Most of the torque comes from orders near $m \sim r\Omega/c$, for which the ratio becomes $\sim\sigma_2/f_{\rm D}T_2^3 \sim O(1)$ with the values adopted here (see Section IIIa). This suggests that fairly similar torque density functions apply to both planet and disk and that such calculations do offer insight into the behavior of the disk–protoplanet system, providing a baseline for further investigations. The ramifications of relaxing the local damping assumption is discussed briefly in Section IVb and will be the subject of a follow-up paper. Other planned extensions of the present work are discussed in Section IVc.

III. STEADY-STATE MIGRATION

In this section, we consider a model problem that illustrates under what conditions a perturber executes either type I or type II drift. The equation of motion for the disk is obtained by including the torque density in the usual fluid equation for a viscous disk (Lynden-Bell and Pringle 1974, Hourigan and Ward 1984, Ruden and Lin 1986, Ruden and Pollack 1991),

$$2\pi r\sigma\frac{DH}{Dt} = -\frac{\partial g}{\partial r} + \frac{dT}{dr}, \tag{16}$$

where $H \equiv r^2\Omega$ is the specific angular momentum of disk material, $g \equiv -2\pi\sigma\nu r^3\partial\Omega/\partial r$, is the viscous couple, ν denotes the kinematic viscosity and $D/Dt \equiv \{\partial/\partial t + v\partial/\partial r\}$ represents the convective derivative, with $v(r)$ being the radial velocity of disk material. The continuity equation reads

$$\frac{\partial\sigma}{\partial t} + \frac{1}{r}\frac{\partial}{\partial r}(r\sigma v) = 0. \tag{17}$$

The motion of the secondary that results from the net tidal torque must be determined by integrating the torque density over the disk,

$$v_{\rm s} = \frac{2}{Mr_{\rm s}\Omega_{\rm s}}\int -\left(\frac{dT}{dr}\right)dr. \tag{18}$$

A solution is sought in which the surface density is in the form of a *kinematic* wave that tracks the planet: $\sigma = \sigma(r - v_{\rm s}t)$. We adopt the $(k, l) = (0, 1)$ disk of Fig. 1 as the unperturbed state, for which $h' \equiv h/r = constant$, $\sigma_0 = constant$. In terms other than the torque density, we set $\Omega = \Omega_{\rm K}$, and $\nu = \alpha h_{\rm s}^2\Omega_{\rm s}$. Euler's equation becomes

$$3\pi\nu r^2\Omega\frac{\partial\sigma}{\partial r} + \pi\sigma r^2\Omega(v + 3\nu/2r) = \frac{dT}{dr}. \tag{19}$$

We now ignore slow changes where $d/dr \sim 1/r$ and define the nondimensional quantities: $\hat{\sigma} \equiv \sigma/\sigma_0$, $\hat{v}_{\rm i} \equiv v_{\rm i}/r_{\rm s}\Omega_{\rm s}$, $\hat{\nu} \equiv \nu/r_{\rm s}^2\Omega_{\rm s}$, $x \equiv (r - r_{\rm s})/h_{\rm s}$, $\hat{t} \equiv \Omega_{\rm s}t$. Equations (16), (17), and (18) simplify to

$$\frac{3\hat{\nu}}{h'}\frac{\partial\hat{\sigma}}{\partial x} + \hat{\sigma}(\hat{v} + 3\hat{\nu}/2) = \frac{\mu^2}{h'^4}\hat{\sigma}F(x, k, l) \tag{20}$$

$$\frac{\partial\hat{\sigma}}{\partial\hat{t}} + \frac{1}{h'}\frac{\partial}{\partial x}(\hat{\sigma}\hat{v}) = 0 \tag{21}$$

$$\hat{v}_{\rm s} = -\frac{2\mu\mu_{\rm g}}{h'^3}\int\hat{\sigma}F(x)\,dx, \tag{22}$$

with

$$F(x,k,l) = \frac{dT/dr}{\mu^2\pi\sigma r_s(r_s\Omega_s)^2/h_s'^4} = \frac{\varepsilon(2/\pi)\xi^4\psi^2\alpha^2}{(1+4\xi^2)}. \quad (23)$$

The assumed kinematic wave form implies that $\partial\hat{\sigma}/\partial t = -v_s\partial\hat{\sigma}/\partial r$ and from the continuity equation, $\hat{\sigma}(\hat{v} - \hat{v}_s) = constant.$ The quantity, $2\pi\sigma r(v - v_s)$ is the flux of disk material seen in the moving frame of the secondary. Evaluated far from the secondary where the disk velocity should be undisturbed, we expect $\sigma(v - v_s) \to -\sigma_o(3\hat{\nu}/2 + v_s)$, so the replacement $\hat{\sigma}\hat{v} \to (\hat{\sigma} - 1)\hat{v}_s - 3\hat{\nu}/2$ can be made in the equation of motion to give

$$\frac{3\hat{\nu}}{h'}\frac{\partial\hat{\sigma}}{\partial x} + (\hat{\sigma} - 1)(\hat{v}_s + 3\hat{\nu}/2) = \frac{\mu^2}{h'^4}\hat{\sigma}F(x,k,l). \quad (24)$$

Equation (24) is nonlinear because of the resonance shifts on the right-hand side (RHS) through $k(\hat{\sigma})$. If we evaluate F with the unperturbed surface density, $F \to F(x, 0, 1) \equiv F(x)$, the resulting linear equation is easily solved. The form function, $F(x)$ is simply that of figure 4, and while its use introduces some error in the determined surface density perturbation, ignoring the pressure buffer in the tidal response of the nebula is not a severe distortion of the net torque unless there is a pronounced gap.

a. Inviscid Disk

Since diffusion tends to impede gap formation, setting ν to zero will establish a lower bound on the mass that can open a gap. Equation (24) gives

$$\hat{\sigma} = (1 - \mu^2F/h'^4\hat{v}_s)^{-1}, \quad (25)$$

which can be substituted into Eq. (22) and integrated, yielding

$$\begin{aligned}\hat{v}_s &= -\frac{2\mu\mu_g}{h'^3}\int_{-\infty}^{\infty}\frac{F\,dx}{1 - \mu^2F/h'^4\hat{v}_s} \\ &\approx -\frac{2\mu\mu_g}{h'^3}\Gamma_1 - \frac{2\mu^3\mu_g}{\hat{v}_s h'^7}\Gamma_2 - \cdots,\end{aligned} \quad (26)$$

where $\Gamma_n \equiv \int_{-\infty}^{\infty}F^n(x)\,dx$, $n > 0$. The first term of the expansion on the RHS is the direct driving by tides from the unperturbed disk. The following terms represent "indirect" driving due to the tidal adjustment of the disk. The solution to lowest order,

$$\hat{v}_s = -\frac{\mu\mu_g}{h'^3}\Gamma_1(1 \pm \sqrt{1 - \mu/\mu_i}), \quad (27)$$

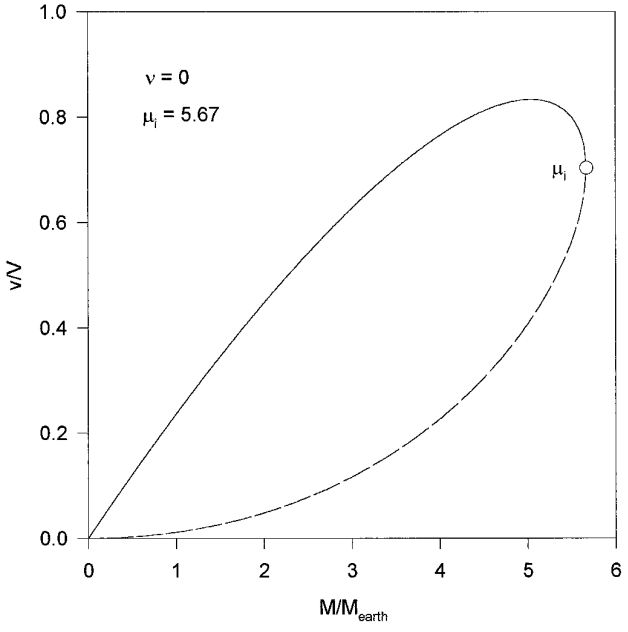

FIG. 5. Drift velocity for an inviscid disk. There is both a stable and an unstable branch merging at a critical mass (inertial limit) $\mu_i = 5.67\ \mu_\oplus$. For $\mu \ll \mu_i$, the velocity is proportional to mass on the stable branch. As the mass approaches the inertial limit, the drift rate stalls and a crisis develops. For larger masses, no steady-state solution exists and the perturber opens a gap in the disk.

can be written in terms of the so-called inertial limit (Hourigan and Ward 1984, Ward and Hourigan 1989),

$$\mu_i \equiv \mu_g h'\Gamma_1^2/2\Gamma_2. \quad (28)$$

The quantity Γ_1 is a measure of the net disk torque and its value can be obtained by summing over the torques as in Section II, for which $\Gamma_1 = 0.248$. Similarly, the parameter Γ_2 is found from the sum,

$$\Gamma_2 = h_s\sum\hat{T}_m^2\left|\frac{dm}{dr}\right| = h_s\sum\frac{m\hat{T}_m^2}{2\kappa^2}\left|\frac{dD_*}{dr}\right|, \quad (29)$$

which gives $\Gamma_2 = 0.443$. Since $\Gamma_1 > 0$, the orbits decay, $\hat{v}_s < 0$. The solution is plotted in Fig. 5. In this and subsequent plots, it is convenient to ratio velocities to the value

$$V \equiv -\frac{2\mu_\oplus\mu_g}{h_s'^3}, \quad (30)$$

where $\mu_\oplus \equiv M_\oplus/M_p$, $M_\oplus = 6 \times 10^{27}$ g denoting an Earth mass. Only the positive branch is stable; the inertial limit gives the maximum mass for which a quasi-steady-state drift solution exists for an inviscid disk. Larger masses will

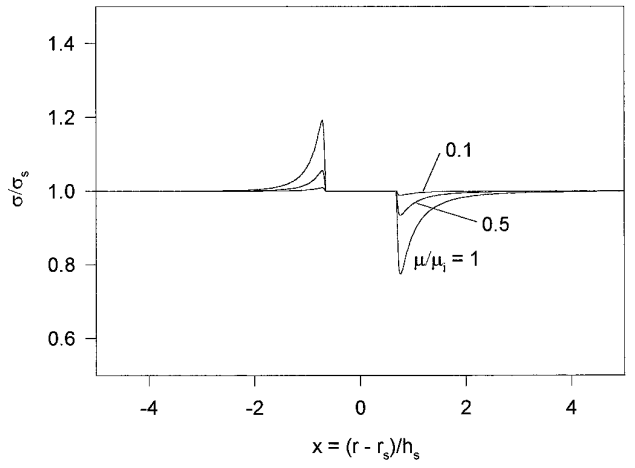

FIG. 6. Surface density perturbation in an inviscid disk as a function of distance for various mass perturbers. Distance is measured in scale heights; mass is indicated as a fraction of the inertial mass. The motion of the protoplanet is to the left so that a density maximum (minimum) leads (trails) the object. This adjustment of the disk to the tidal torque causes a feedback torque (indirect driving) that opposes the motion. At the inertial limit, the feedback is sufficient to cause stalling.

stall and open a gap. Substituting Eq. (27) into (25) gives the surface density perturbation,

$$\hat{\sigma} \approx 1 - \frac{1}{2}\left(\frac{\Gamma_1}{\Gamma_2}\right)(1 - \sqrt{1 - \mu/\mu_i})F(x), \tag{31}$$

as a function of perturber mass. Figure 6 shows the surface density for several values of μ/μ_i. The motion is to the left so that a density enhancement (depletion) leads (trails) the object located at $x = 0$. This produces the disk's feedback torque that tries to resist the object's advance. The larger the perturber, the more pronounced the effect becomes. At the critical mass, there is a crisis; the migration stalls and a gap commences to form. The steepness of the density perturbation nearest the perturber is due to the torque cutoff, but is artificial since pressure effects that would soften this feature as discussed by Hourigan and Ward (1984) have been ignored, and a steep surface density gradient, i.e., $>O(\sigma/h)$, would be Rayleigh unstable (e.g., Lin and Papaloizou 1993). As we shall show below, viscous diffusion will also spread out abrupt density differences. As an application, consider a protoplanet at an orbital distance of 5 AU in a circumstellar nebula with a normalized scale height $h/r \sim 0.07$ for which $\mu_g \sim 3.5 \times 10^{-3}$, which is considered appropriate for the jovian zone in a minimum mass solar nebula. The characteristic drift time corresponding to the normalization rate, Eq. (30), is $\tau \equiv (\Omega V)^{-1} = 2.9 \times 10^4$ years. Equation (28) yields $\mu_i \approx 1.7 \times 10^{-5}$; assuming a one solar mass primary, $M_i \sim 6$ Earth masses. The characteristic orbital drift time, $\tau \equiv r/v_s = (\hat{v}_s\Omega)^{-1}$, for such an object is less than 10^5 years.

b. Weak Viscosity

If $\nu \neq 0$, the general solution to equation (24) reads

$$\hat{\sigma} = 1 + \beta e^{\beta\Gamma(x)+\gamma x}\int_{\infty}^{x} F(y)e^{-\beta\Gamma(y)-\gamma y}\,dy, \tag{32}$$

where

$$\Gamma(x) \equiv \int_0^x F(x)\,dx; \qquad \beta \equiv \frac{\mu^2}{3\hat{\nu}h'^3}; \qquad \gamma \equiv -\frac{h'}{3\hat{\nu}}(\hat{v}_s + 3\hat{\nu}/2). \tag{33}$$

Substitution into Eq. (22) then yields an integral equation for the velocity of the secondary,

$$\hat{v}_s = -\frac{2\mu\mu_g}{h'^3}\Gamma_1 - \frac{2\mu\mu_g}{h'^3}\int_{-\infty}^{\infty} F(x)e^{\beta\Gamma(x)+\gamma x} \int_{\infty}^{x} \beta F(y)e^{-\beta\Gamma(y)-\gamma y}\,dy\,dx. \tag{34}$$

If $\gamma \gg 1$, the integrand of the y-integral will not vary much before it is suppressed by the factor $e^{-\gamma(y-x)}$. In this case, the remaining portion, $-\beta F(y)e^{-\beta\Gamma(y)} = (d/dy)e^{-\beta\Gamma}$, can be expanded in a Taylor series. The interior integral then yields

$$\int_x^{\infty} \beta F(y)e^{-\beta\Gamma(y)}e^{-\gamma(y-x)}\,dy = \sum_{n=1}\frac{1}{\gamma^n}\frac{d^n}{dy^n}e^{-\beta\Gamma(y)}\Big|_x. \tag{35}$$

Substituting into Eq. (34) and integrating gives

$$\hat{v}_s = -\frac{2\mu\mu_g}{h'^3}\left[\Gamma_1 - \frac{\beta}{\gamma}\left(\Gamma_2 - \frac{\beta}{\gamma}\Gamma_3 + \left(\frac{\beta}{\gamma}\right)^2\Gamma_4 + \cdots\right) - \frac{\Lambda_2}{\gamma^2} + \cdots\right], \tag{36}$$

where $\Lambda_n = \int_{-\infty}^{\infty}(dF/dx)^n\,dx$. Note that in the limit $\nu \to 0$, $\gamma \to \infty$; $\beta/\gamma = -\mu^2/\hat{v}_s h'^4$, and we recover the inviscid solution Eq. (26).

c. Strong Viscosity

The normalized torque density, $F(x)$, falls off rapidly for $|x| > 1$. Hence, if, $\gamma \ll 1$, we can expand Eq. (32) to first order in γ, to find

$$\hat{\sigma} \approx e^{-\beta(\Gamma(\infty)-\Gamma)} - \gamma x(1 - e^{-\beta(\Gamma(\infty)-\Gamma)}) - \gamma\beta e^{\beta\Gamma}\int_{\infty}^{x} yF(y)e^{-\beta\Gamma(y)}\,dy. \tag{37}$$

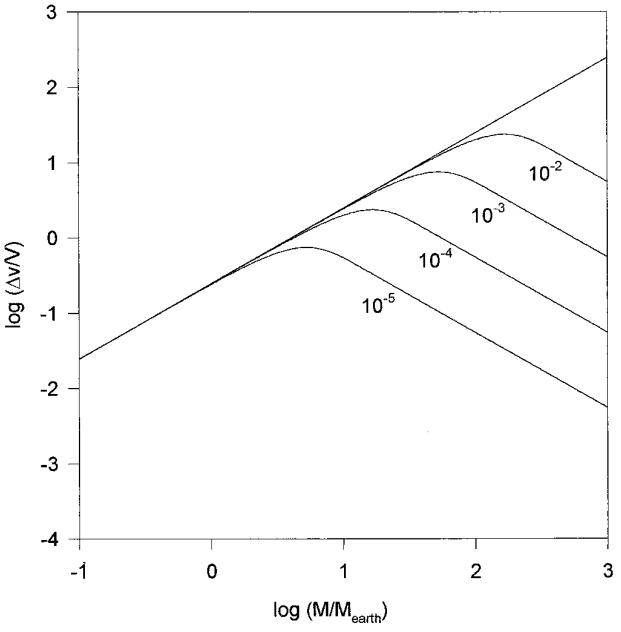

FIG. 7. Disk torque exerted on a perturber comoving with the disk viscous flow, $\gamma = 0$. Torque strength is measured by the equivalent drift velocity, Δv_s, it could produce if acting alone. There is a maximum value at $\mu_\nu\sqrt{1.26/\Gamma_1} = 2.25\mu_\nu$, where $\mu_\nu \equiv 3(\nu/r^2\Omega)(h/r)^3$ is the so-called viscous mass.

Substitution into (22) and integrating by parts yields

$$\hat{v}_s = -\frac{2\mu\mu_g}{h'^3}\left[\frac{1 - e^{-\beta\Gamma_1}}{\beta} - \gamma\beta I(\beta)\right], \tag{38}$$

where

$$I(\beta) = \frac{1}{\beta}\int_{-\infty}^{\infty} xF[e^{\beta(\Gamma(-\infty)-\Gamma)} - e^{-\beta(\Gamma(\infty)-\Gamma)}]\,dx. \tag{39}$$

First consider the case $\gamma = 0$. This is equivalent to assuming the protoplanet does not drift *relative* to the ambient disk flow, i.e., $\hat{v}_s = -3\hat{\nu}/2$. The first term in Eq. (38) then gives the contribution, $\Delta\hat{v}_s$, of the disk torque to $\hat{v}_s$. (Since $\Delta\hat{v}_s$ is generally not equal to $-3\nu/2$, an additional torque would have to be applied to maintain $\gamma = 0$.) Defining a viscous mass,

$$\mu_\nu \equiv (3\hat{\nu}h'^3)^{1/2} = 2.24 \times 10^{-3}\sqrt{\alpha} \tag{40}$$

(where the numerical values apply to a $h' = 0.07$ disk), this can be written

$$\Delta\hat{v}_s = -\frac{2\mu_g\mu_\nu^2}{h'^3\mu}(1 - e^{-\Gamma_1(\mu/\mu_\nu)^2}). \tag{41}$$

This quantity, normalized to V, is plotted in Fig. 7 for various values of α. Equation (41) has a maximum at $\mu = \mu_\nu\sqrt{1.26/\Gamma_1} = 2.25\mu_\nu$.

Next let $\gamma \neq 0$, $\beta \ll 1$. The limit of Eq. (39) as $\beta \to 0$ is

$$I(0) = \int_{-\infty}^{\infty} xF(x)[\Gamma_0 - 2\Gamma(x)]\,dx, \tag{42}$$

where $\Gamma_0 \equiv \Gamma(\infty) + \Gamma(-\infty) = \Sigma\,|\hat{T}_m| = 0.792$. Using the ansatz torque density described below, this quantity can be approximated as $I(0) \approx 0.25$. Defining an auxiliary mass

$$\mu_* = \mu_\nu\left(\frac{\mu_\nu}{2I\mu_g h'}\right)^{1/3} = 3.71 \times 10^{-3}\alpha^{2/3}/I^{1/3}, \tag{43}$$

Eq. (38) can be rewritten as

$$\hat{v}_s = \frac{\Delta\hat{v}_s}{1 + (\mu/\mu_*)^3} - \frac{3\hat{\nu}/2}{1 + (\mu_*/\mu)^3}. \tag{44}$$

This solution is plotted in Fig. 8 for the same values of α used in Fig. 7 and with $I = I(0)$. The second term in Eq. (44) causes v_s to reduce to $v_s = -(3/2)\hat{\nu}(r\Omega) = -(3/2)\alpha(r\Omega)(c/r\Omega)^2$ as $\mu \to \infty$, revealing $c_2 = -3/2$ in Eq. (2) for type II motion in the disk's interior.[7] However, as

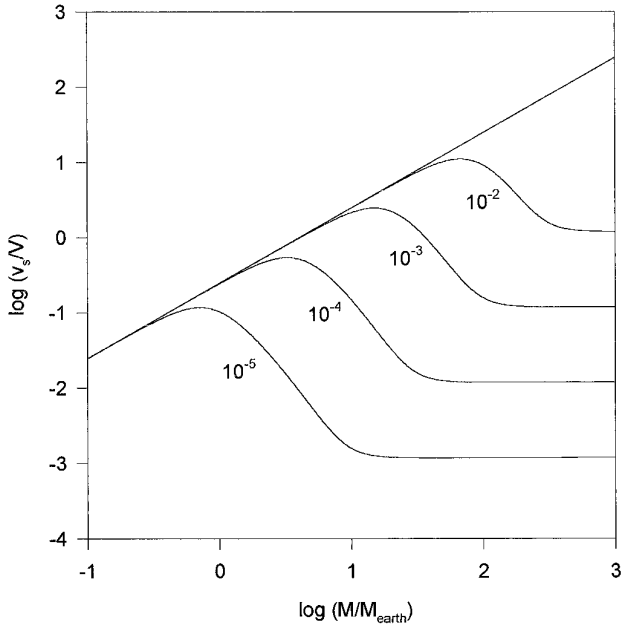

FIG. 8. Drift velocity as a function of mass predicted by strong viscosity approximation Eq. (44). Velocities are normalized to $V \equiv -2\mu_\oplus\mu_g r\Omega/h_s'^3$ and mass is in Earth masses.

[7] This value of c_2 pertains only to our assumed case of a constant surface density and viscosity. In a realistic disk with an outer boundary, the most remote portions spread outward so that $c_2(r)$ turns positive in that region (e.g., Lynden-Bell and Pringle 1974).

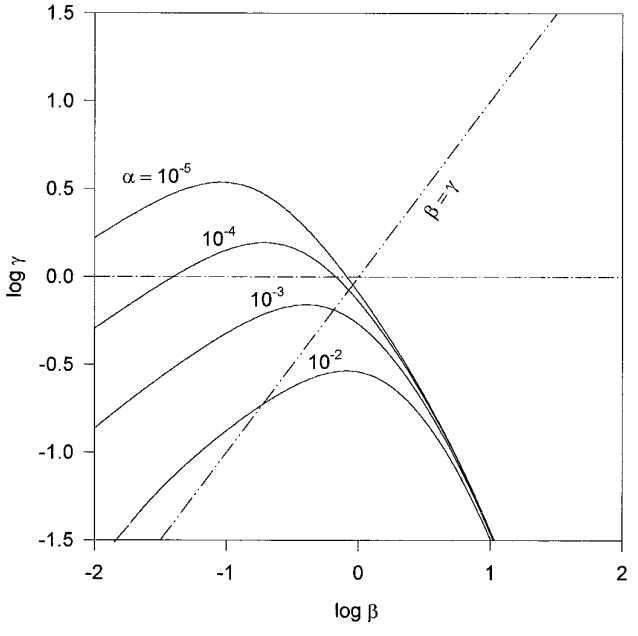

FIG. 9. Relative drift parameter, $\gamma \equiv -(h'/3\hat{r})(\hat{v}_s + 3\hat{r}/2)$, as a function of $\beta \equiv (\mu/\mu_\nu)^2$ for strong viscosity approximation. Protoplanet locks into disks flow (type II) as $\gamma \to 0$. Portion of curves for which $\gamma > 1$ are invalid because they violate the assumptions underlying the approximation.

$\mu \to 0$, Eq. (44) reads $v_s = -2\Gamma_1\mu(r\Omega)(\pi\sigma r^2/M_p)(r\Omega/c)^3$, so that the constant of Eq. (1) for type I motion becomes $c_1 = -2\pi\Gamma_1 = -1.56$. Note that the first term of Eq. (44) contains the additional factor, $[1 + (\mu/\mu_*)^3]^{-1}$, which shifts the maximum to lower mass ($\approx\mu_*$) if $\mu_*/\mu_\nu = (\mu_\nu/2Imu_g h')^{1/3} = 1.65\alpha^{1/6}/I^{1/3} < 1$.

From the definition Eq. (33),

$$\gamma = -\frac{h'}{3\hat{r}}\left(\frac{\Delta\hat{v}_s + 3\hat{r}/2}{1 + (\mu/\mu_*)^3}\right), \tag{45}$$

which goes to zero as $\mu \gg \mu_*$ (Fig. 9). Remembering that γ is proportional to the drift of the protoplanet *relative* to the disk, we again see that large objects tend to lock into the disk. However, Eq. (44) is derived under the assumption that $\gamma \ll 1$, a condition violated by portions of the $\alpha = 10^{-4}, 10^{-5}$ curves in Fig. 9. Accordingly, the corresponding curves near their maxima in Fig. 8 are suspect. In the next section, we find these curves by a numerical integration.

d. Moderate Viscosity

For intermediate values of the viscosity, Eq. (34) can be evaluated by numerical integration. Notice, however, that the procedure involves a triple integration by virtue of the definition, $\Gamma(x) \equiv \int_0^x F(x)\,dx$. On the other hand, we should recall that Eq. (23) is not the true torque density anyway, but a smoothed average that does not actually follow the variations of the torque during the driving of the waves. Furthermore, at the level of accuracy at which we are working, $F(x)$ is being treated as a fixed form factor, ignoring any modification through pressure gradient effects. This suggests we might replace the rather complex torque density of Eq. (23) with a simpler form that displays that same general behavior, but is integrable in closed form. At this level of approximation, the additional uncertainly introduced by such an *ansatz* form factor is relatively minor, and we are compensated by the increased economy of evaluating Eq. (34). We adopt

$$F(x) \equiv \varepsilon e^{-|d/z|}\left(\frac{A}{z^4} + \frac{B}{z^3}\right); \qquad |x| > 2/3, \tag{46}$$

for which

$$\Gamma(x) = e^{-|d/z|}\left[\frac{A}{d^3}\left(2 + 2\left|\frac{d}{z}\right| + \left(\frac{d}{z}\right)^2\right) + \varepsilon\frac{B}{d^2}\left(1 + \left|\frac{d}{z}\right|\right)\right], \tag{47}$$

while for $|x| < 2/3$, $F = \Gamma = 0$. (The rationale for this choice is discussed in Appendix C.) The asymptotic values are $\Gamma(\pm\infty) = 2A/d^3 \pm B/d^2$. The constants A, B, d are now selected to duplicate the integrated values $\Gamma_0 = 0.792$, $\Gamma_1 = 0.248$, $\Gamma_2 = 0.443$, respectively. For the $k = 0$, $l = 1$ disk, the values are $A = 0.228$, $B = 0.136$, $d = 1.05$. Figure

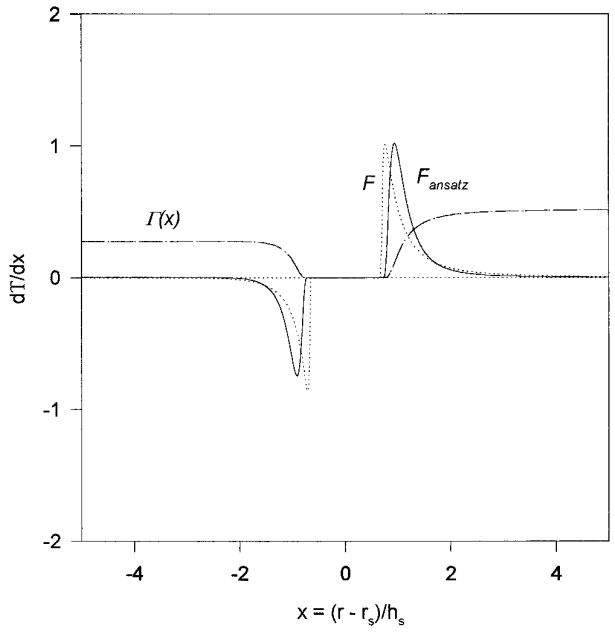

FIG. 10. Comparison of ansatz torque density, $F_{ansatz}(x)$, to smoothed torque density, $F(x)$. Also shown is $\Gamma(x)$, which can be written in closed form for the ansatz function.

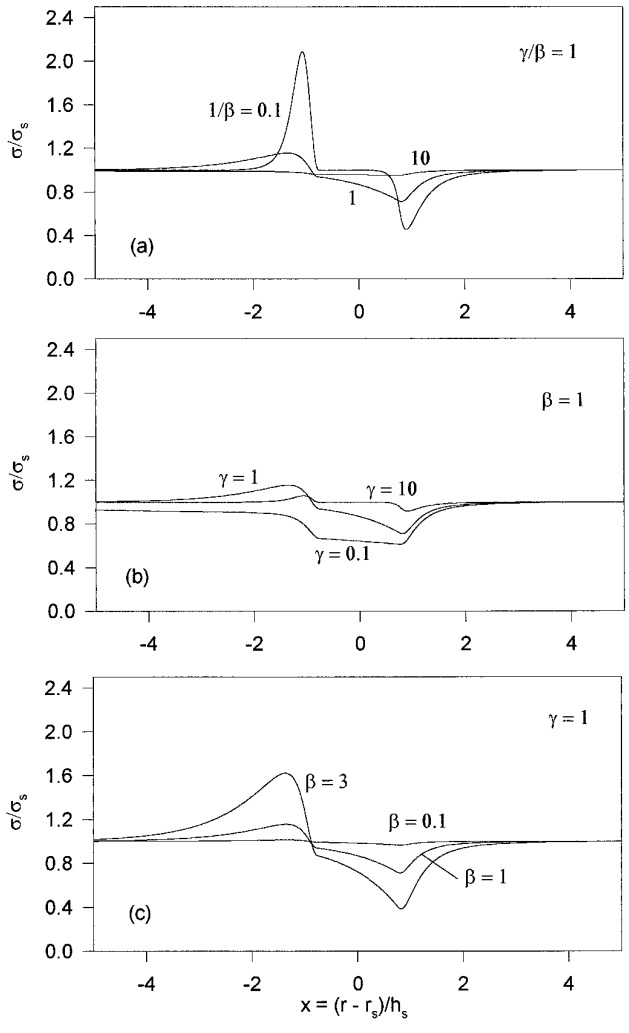

FIG. 11. Surface density perturbation for (a) constant mass and drift velocity, but increasing viscosity, (b) constant mass and viscosity, but increasing drift velocity, and (c) constant drift velocity and viscosity, but increasing mass. Distances are shown in units of scale height. Densities are normalized to unperturbed value.

10 displays Eqs. (46) and (47) for comparison with Eq. (23). Equation (46) retains the essential asymmetry of the torque as well as its qualitative behavior at small and large x.

Equation (32) is now easily integrated to find the surface density as a function of $\{\beta, \gamma\}$, and to explore the influence of the different parameters on the nature of the density perturbation. Figure 11a shows the effect of increasing the viscosity. At low viscosity, the density profile resembles the inviscid case. As the viscosity is increased, the perturbation is progressively suppressed. This diminishes the indirect torque and helps prevent stalling. In Fig. 11b, the viscosity of the disk and the mass of the perturber are fixed, but the relative velocity is varied through γ. A rapid velocity allows less time for a significant density perturbation to develop, while a low relative velocity results in the development of a gap. Figure 11c shows the result of increasing the perturber's mass while maintaining constant relative velocity and disk viscosity. For large enough objects, a density perturbation develops that is comparable to that in the critical inviscid case, and stalling occurs.

Equation (22) is easily solved by iteration. We first renormalize the velocity in a slightly different manner; $\tilde{v}_s \equiv \hat{v}_s / V_\nu$, where

$$V_\nu \equiv -\frac{2\mu_g \mu_\nu}{h'^3}. \tag{48}$$

Then Eq. (22) reads

$$\tilde{v}_s(\beta, \gamma) = \sqrt{\beta} \int \hat{\sigma} F \, dx. \tag{49}$$

The behavior of $\tilde{v}_s(\beta, \gamma)$ is shown in Fig. 12. This quantity is a measure of the total driving of the disk, including both direct and indirect contributions. On the other hand, from the definition of γ,

$$\tilde{v}_s(\alpha, \gamma) = \frac{1}{2h'} \left(\frac{\mu_\nu}{\mu_g}\right) \left(\gamma + \frac{h'}{2}\right) = \frac{\sqrt{3\alpha h'^3}}{2\mu_g} \left(\gamma + \frac{h'}{2}\right). \tag{50}$$

Representative curves are included in Fig. 12. A self-con-

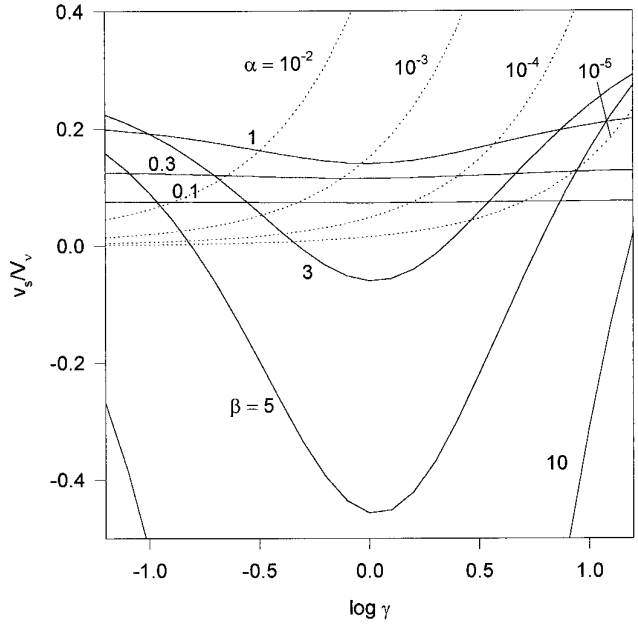

FIG. 12. Comparison of driven velocity, $\tilde{v}_s(\beta, \gamma)$, with assumed velocity, $\tilde{v}_s(\alpha, \gamma)$, which correspond to RHS and LHS of Eq. (34), respectively. Intersections of the curves give the solutions $\gamma(\alpha, \beta)$.

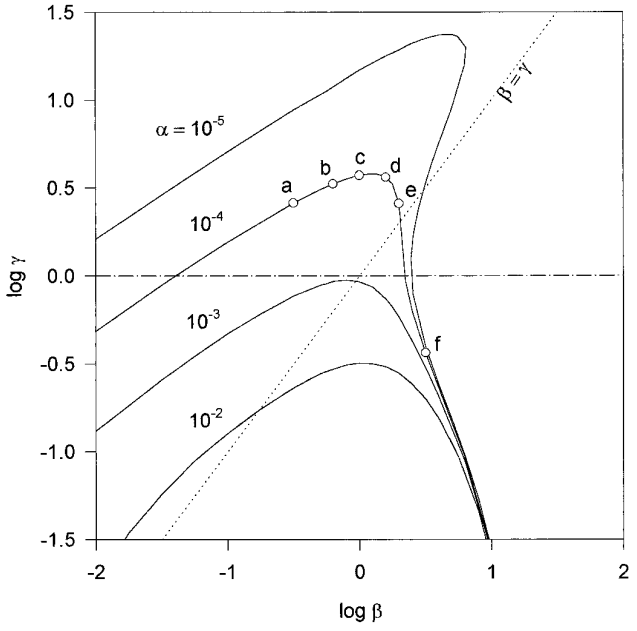

FIG. 13. Solutions to integral equation for the drift velocity giving the relative velocity parameter, γ, as a function of mass through $\beta \equiv (\mu/\mu_\nu)^2$. The points on the $\alpha = 10^{-4}$ curve corresponds to the density plots in Fig. 15. Note that the curves for $\alpha = 10^{-5}$, 10^{-4} curves differ markedly from those of Fig. 8. For these curves, the motion of the protoplanet is more important than the viscosity in preventing the formation of a gap.

sistent solution requires $\tilde{v}_s(\alpha, \gamma) = \tilde{v}_s(\beta, \gamma)$, from which we obtain $\gamma(\alpha, \beta)$ by iteration. These solutions are plotted in Fig. 13 for several values of α. As expected, portions of the curves above $\gamma = 1$ are considerably modified from those in Fig. 9. These portions tend to follow the inviscid solution whenever it predicts a larger value of $\hat{v}_s$ than Eq. (44), i.e., when $\mu_i > \mu_*$. This implies that inertial effects are more important than viscosity at preventing gap development for these values of α. Figure 14 displays the corresponding velocities normalized to V. The conversion from type I to type II migration occurs more steeply with mass than in Fig. 8, particularly at low viscosity. Any portions of the curves, such as for $\alpha = 10^{-5}$, that are triple valued in velocity for a given mass are unstable at the intermediate value. This is similar to the unstable branch of the inviscid curve of Fig. 5. The reason can be understood by inspection of Fig. 12. When, for a given pair (α, β), the two velocity curves intersect at a single point, the slope of $\tilde{v}_s(\alpha, \gamma)$ is greater than that of $\tilde{v}_s(\beta, \gamma)$ (e.g., curve $\alpha = 10^{-4}$ with curve $\beta = 3$ near $\log \gamma = -0.4$) and the equilibrium is stable, since a small displacement in velocity (or γ) creates disk conditions that tend to return the protoplanet to its original state. By contrast, when the velocity curves intersect in three places, the slope of $\tilde{v}_s(\alpha, \gamma)$ is less than the slope of $\tilde{v}_s(\beta, \gamma)$ at the intermediate value of γ (e.g., the intersection of curve $\alpha = 10^{-5}$ with curve $\beta = 3$ near $\log \gamma = 0.4$). A small displacement of the state toward higher (lower) velocity will create conditions that produce stronger (weaker) driving than required to maintain the state. The velocity will accelerate (decelerate) until it encounters the next intersection, which will then be a stable equilibrium.

IV. DISCUSSION

a. Cosmogonical Implications

Any mechanism that could affect the radial distribution of mass in an accreting planetary system could have important consequences for the style and time scale of planet formation. Except for the influence of aerodynamic drag, which loses its effectiveness for planetesimals larger than a few kilometers, most models of the planetesimal disk assume that the primary cause of radial migration is mutual scattering (e.g., Hayashi *et al.* 1977, Wetherill 1990). The possibility that nebula torques could have provided radial mobility to large, planetary sized objects introduces another degree of freedom in accretion modeling (e.g., Hourigan and Ward 1984, Ward 1989, 1993, Ward and Hahn 1995). To date, this suggestion has received limited attention by the planetary science community (e.g., Wetherill 1990, Lissauer and Stewart 1993, Korycansky and Pollack 1993, and Artymowicz, 1993a,b). This may be rooted in a caveat stated in GT80 that: "With our scant knowledge of the nebula we cannot be certain whether the interior or exterior torque is larger. Thus, we can estimate only the magnitude of the effect, not its sign." This view seems to have persisted in the literature (Lin and Papaloizou 1993; Takeuchi *et al.* 1996) and has, perhaps, discouraged attempts to consider the effects of disk tides on the accretion process. We have found this to be overly pessimistic.

Figure 14 indicates that protoplanets close to the stall point for type I drift migrate at rates between one and two orders of magnitude faster than the disk's viscous drift rate. One apparent misconception is that the torque mismatch is only a very small fraction of the total disk torque (e.g., Lissauer and Cuzzi 1985, Shu *et al.* 1993).[8] We have seen that the protoplanet torques the disk most strongly at distances $\sim \pm h$ from its orbit. Because the nebula is relatively thick, $h/r \sim O(10^{-1})$, there is a wide fractional separation, $\sim 2h/r$, of the peak torquing regions, resulting in a differential that can amount to fair fraction of the whole. For the disk model shown in Fig. 1, the total fractional differential torque, $2|T_{\text{outer}} + T_{\text{inner}}|/(|T_{\text{outer}}| + |T_{\text{inner}}|)$, found by summing over m, is 50%. Furthermore, the torque asymmetry or mismatch is not due solely to poorly constrained density

[8] The ~5% mismatch calculated in GT80 refers to a small dominance of corotation over Lindblad torques in the rate of eccentricity variation, not to the competition between outer and inner Lindblad resonances in changing the semimajor axis.

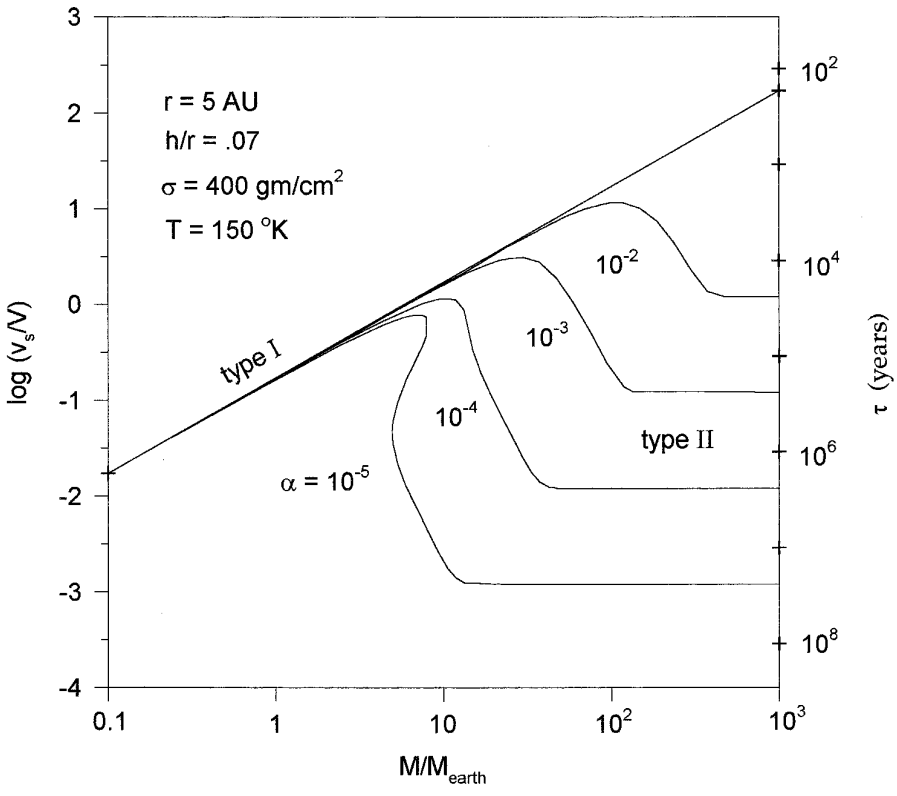

FIG. 14. The drift velocity as a function a mass for various values of the viscosity parameter, α. Assumed conditions are considered appropriate for the jovian zone in a minimum mass solar nebula. Transition from type I to type II motion is accompanied with a substantial drop in velocity. For modest values of the viscosity, the threshold mass is comparable to a giant planet core. Characteristic drift times for threshold objects are typically much shorter than the lifetime of the gas disk.

and temperature gradients of the disk as implied in GT80 and, more recently, by Lin and Papaloizou (1993). There are intrinsic asymmetries in the forcing function and resonance positions that contribute. The decrease of the disk's epicycle frequency with heliocentric distance is also an important factor. Indeed, the torques shown in Fig. 1 are for a *constant* density disk. Global gradients in the disk turn out to be less important than originally thought because of a "buffering" action between the density gradient and its associated pressure gradient (Ward 1986, Korycansky and Pollack 1993).

We also believe that the sensitivity of the net torque to local disk structure in the case of the solar nebula has been exaggerated. This attitude may in part be due to the planetary community's experience with particle rings. Torques from extremely thin structures such as Saturn's rings *are* strongly controlled by local conditions and can be significantly changed by the rearrangement of a relatively small amount of disk material close to the perturber (e.g., Lissauer and Cuzzi 1985). However, this is much less the case for the solar nebula where the amount of strongly interacting disk material is of order $\sim 4\pi r\sigma h$. For a minimum mass solar nebula at $r \sim 5$ AU, this is of order 10^{30} g, i.e., a mass comparable to that of Jupiter, which is not so easy to rearrange.

In Fig. 15, we show the surface density for several representative points along the $\alpha = 10^{-4}$ curve of the velocity diagram. Curves a–c show the surface signature typical of an object executing type I drift. The direction of motion is to the left. For $\beta = 1$ (curve c), the perturbation is several percent and the leading maximum and trailing minimum are well developed. Detection of this type of feature would furnish possible evidence of rapidly migrating objects embedded in the disk. At $\beta = 1.6$ (curve d), the indirect driving contribution due to the density perturbation is large enough to start slowing the drift rate. For still larger masses (curves e–f), a gap progressively opens and locks the perturber into the disk and type II behavior. The conditions depicted in Figs. 15a–15f are indicated on the $\alpha = 10^{-4}$ curve in Fig. 13. The value of $\gamma = 10^{.572} = 3.73$ used in Fig. 15c implies a drift velocity $\hat{v}_s = -(3\hat{v}/2)(\gamma/h' + 1) \approx 52\hat{v}_g$, where $\hat{v}_g$ represents the viscous flow rate of the unperturbed disk. Interestingly, Fig. 14 indicates that the most mobile objects for turbulent viscosities believed relevant to the solar nebula (i.e., $\alpha \sim 10^{-4}$–10^{-3}) are those with masses comparable to giant planet cores (i.e., 10–30

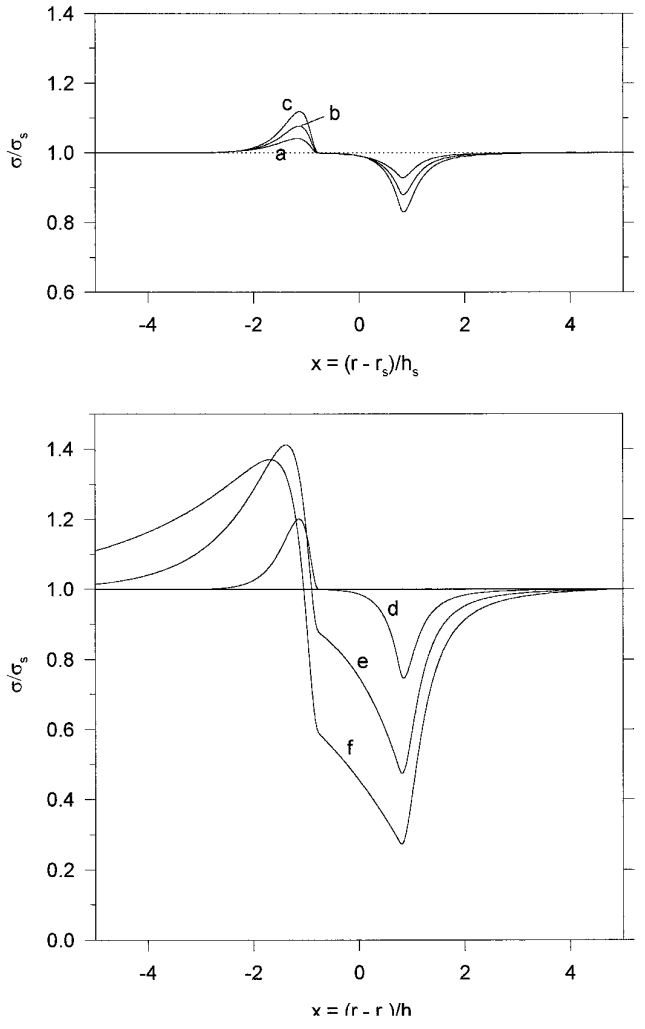

FIG. 15. Surface density configuration associated with the positions indicated on the $\alpha = 10^{-4}$ curve of Fig. 12. Masses approaching the threshold value (a–c) show increased amplitude of kinematic wave form tracking the planet during type II drift. For masses in excess of the threshold (d–f), the disturbance progressively takes the form of a gap, which locks the perturber to the disk and completes the transition to type II motion.

$M_\oplus$). Both smaller and larger objects drift more slowly. This differential motion may have assisted in late-stage growth, helping to account for the appearance of giant planet cores prior to disk dispersal (e.g., Ward 1989, 1993, Ward and Hahn 1995, Araki and Ward 1995).

At the same time, this mechanism is potentially destructive. If a decaying protoplanet cannot stabilize its orbit in time, it will drift into the primary. In the jovian zone, embryos with masses of order 2–3 $M_\oplus$ are believed to form quickly (i.e., $O(10^5)$ years) via runaway growth (e.g., Wetherill and Stewart 1989, Lissauer and Stewart 1993). Such objects already have orbital lifetimes considerably shorter than the probable lifetime of the disk. Their ultimate survival may then depend on their further growth to the point where they can abort type I drift. Of course, if a protoplanet can achieve critical size for the onset of *gas* accretion, its growth rate will accelerate significantly. In addition, cannibalizing the disk may also produce a gap-like configuration that could slow its migration. These are topics for further research.

Although converting to slower type II migration increases their lifetime, the accompanying formation of a gap would seem to signal a cessation of any gas accretion as well. Figure 14 then indicates that with local damping a rather large $\alpha \geq O(10^{-2})$ is required to account for threshold masses as great as Jupiter and Saturn (e.g., Papaloizou and Lin 1984). On the other hand, Artymowicz and Lubow (1996) have found by numerical modeling that an object confined to a gap may still be fed by gas streams emanating from the gap edges, so further growth may be possible.

Lin and Papaloizou (1993) have claimed that there is also a necessary condition for gap formation; viz., the perturber's Hill sphere radius must be comparable to or greater than the disk's scale height, i.e., $\mu \geq O(h/r)^3$. The rationale for this seems to be an assumption that the Hill radius sets the width of the gap that a perturber attempts to open, and that widths smaller than the disk thickness would be Raleigh unstable. This criterion is then invoked to explain the final masses of the giant planets. While we agree with the Rayleigh stability argument, we see no tendency for perturbers to attempt the opening of such narrow gaps. Rather, in our calculations, the protoplanet attempts to open a gap of width $\sim h$ or larger, regardless of its size. This is because the strongest torques exerted on the disk are at least at that distance from the perturber (e.g., Fig. 4). Indeed, as mentioned in Section IIc, pressure modification of the oscillation frequency of the disk *prevents* Lindblad resonances from lying closer than $\sim 2h/3$ to the protoplanet (e.g. Artymowicz 1993a).[9] We should point out, however, that the criterion $\mu \sim (h/r)^3$ is also the mass for which disk perturbations become nonlinear at launch. To see this, we note that the density perturbation at an mth order resonance is of order $\delta\sigma_m/\sigma \sim \mu(r\Omega/c)^2(mc/r\Omega)^{5/3}$. Most of the torque comes from $m \sim O(r/h)$, for which $\delta\sigma_m/\sigma \sim \mu/h'^2$. The resonances are separated by $\Delta r \sim r/m^2$, so that there are $N \sim h/\Delta r \sim m^2h' \sim 1/h'$ resonances that overlap in the peak launch zone. There, combined density perturbations can reach $\delta\sigma/\sigma \sim N\delta\sigma_m/\sigma \sim \mu/h'^3$. Hence, nonlinearity, $\delta\sigma/\sigma \sim O(1)$, occurs when $\mu_{NL} \sim O(h'^3)$. This may enhance wave damping and, in turn, promote gap formation. Thus, if linear waves damp nonlocally, the necessary condition for gap formation may have some validity, but for a different reason than stated by Lin and Papaloizou.

[9] Corotation resonances are an exception to this, but tend to set disk material into libration on horseshoe orbits rather than clear a gap.

b. Nonlocal Damping

As mentioned in Section IId, this initial study assumes that density waves damp within a short distant of their launch point. Only then is one justified in using the same expression for the torque density in Eqs. (16) and (18). Relaxing this assumption makes gap formation more difficult and extends the mass range for type I migration. In planetary rings, waves are damped efficiently by nonlinear effects and by viscous dissipation (e.g., Goldreich and Tremaine 1978, Shu 1984, Shu *et al.* 1985). However, pressure waves do not windup as fast as gravity waves so that nonlinear effects develop slowly in a non-self-gravitating gas disk (e.g., Ward 1986). If the viscosity is large enough to damp waves locally, it is also large enough to prevent the opening of a gap for all but the largest protoplanets (Ward 1986, Takeuchi *et al.* 1996). More efficacious sources of damping may be radiation damping (Cassen and Woolum 1996) and/or refraction of the waves to high altitude where they can shock dissipate (e.g., Ward 1985, Lin, Papaloizou and Savonije 1990).

If the angular momentum flux of the wave train is transferred to the disk over a finite distance, δ, the torque density in Eq. (24) should be replaced with a distributed form that acknowledges the effective torque density at any point in the disk, F_d, contains contributions from resonances lying closer to the secondary. Assuming that the angular momentum flux decays exponentially, $e^{-|x/\delta|}$, the form factor for the disk becomes

$$F_d(z, \delta) = \frac{\varepsilon}{\delta}\int_0^z F(y)e^{-|z-y|/\delta}\,dy. \tag{51}$$

In the limit $\delta \to 0$, $\delta^{-1}e^{-|z-y|/\delta}$ becomes twice the Dirac delta function, $2\delta(z-y)$, and integrating Eq. (51) recovers $F(x)$. (The factor of 2 is dropped because the integration is only over half of the delta function.) It is also easy to show from Eq. (51) that $\int_{-\infty}^{\infty} F_d\,dz = \int_{-\infty}^{\infty} F\,dz$, so that the area under the curves is independent of δ, as required by conservation of angular momentum. Since the tidal adjustment of the disk will be spread out over a greater area, the amplitude of F_d must decrease with increased damping length. If $\delta \gg 1$, the integrand of Eq. (51) will die from $F(z)$ before the exponent kicks in, and $F_d \approx \varepsilon\Gamma(z)/\delta$ for $|z| \ll \delta$. Figure 16 displays F_d obtained by integration of Eq. (51) for several values of the damping length.

With a longer damping length, the threshold mass should increase as well. This is most easily demonstrated in the inviscid case. In Eq. (26), the indirect driving coefficient becomes

$$\begin{aligned}\Gamma_2(\delta) &= \int_{-\infty}^{\infty} F(z)F_d(z, \delta)\,dz \\ &= \frac{1}{\delta}\int_{-\infty}^{\infty} \varepsilon F(z)e^{-|z/\delta|}\int_0^z F(y)e^{|y/\delta|}\,dy\,dz.\end{aligned} \tag{52}$$

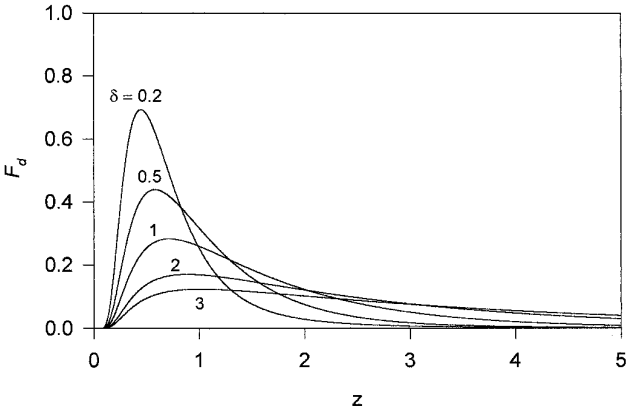

FIG. 16. The normalized disk torque density, $F_d(z)$, for various wave damping lengths.

Substituting the $\delta \gg 1$ approximation, Eq. (52) integrates to $\Gamma_2 \approx [\Gamma(\infty)^2 + \Gamma(-\infty)^2]/2\delta = 0.171/\delta$. From Eq. (28), the inertial mass becomes, $\mu_i \approx 14.6\delta\mu_\oplus$. The peak amplitude of the kinematic wave [Eq. (31)] becomes independent of the damping length; $\Delta\hat{\sigma}_{\max} \approx \Gamma_1 F_{\mathrm{d,max}}/2\Gamma_2 \to 0.376$. Figure 17 shows Γ_2 as a function of damping length found by numerical integration, along with the inertial mass. We see that μ_i grows by a factor of $\sim$3 for $\delta = h$ and up to core size for $\delta \gtrsim 2h$, attaining values comparable to the threshold mass for $\alpha = 10^{-3}$ in the local damping model.

An exponential power, $-|z-y|^n/\delta^n$, that is linear ($n = 1$) seems roughly appropriate for radiation damping. Other

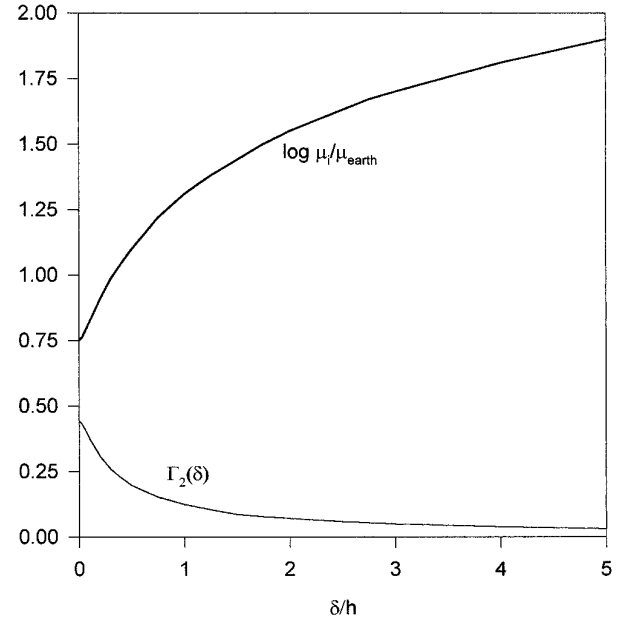

FIG. 17. The coefficient of the disk feed back, Γ_2, and the inertial mass, μ_i, as a function of damping length.

damping mechanisms are better represented by higher n for which the wave travels closer to δ before damping becomes important. This further weakens the feedback torque from the disk and also increases the threshold mass. The disk form factor becomes

$$F_d(z, \delta) = \frac{\varepsilon n}{\delta^n} \int_0^z F(y)(z - y)^{n-1} e^{-|z-y|^n/\delta^n}\, dy. \quad (53)$$

In the case of viscous damping, $n = 3/2$, and $\delta_\nu \approx m^{-1/3}(c^2/\nu\Omega)^{2/3}(c/r\Omega)^{2/3} \approx \alpha^{-2/3}(c/r\Omega)$, where in the last expression the value $m \sim (r\Omega/c)$ for the most important orders has been substituted. However, if viscous damping is important, the inviscid equation for the inertial mass cannot be used. We defer analysis of this case to a subsequent work.

Still higher n would be appropriate for nonlinear shocking of the waves, where the onset of dissipation is more sudden. In the limit $n \to \infty$, $e^{-|z-y|^n/\delta^n} \to 1 - H_S(|z - y| - \delta)$, where H_S represents the Heaviside step function. Its derivative is the Dirac delta function so that

$$F_d(z, \delta) = \varepsilon \int_0^z F(y)\delta(|z - y| - \delta)\, dy = F(z - \varepsilon\delta), \quad (54)$$

which describes a pure translation of the form factor away from the perturber, and

$$\Gamma_2 = \int_{-\infty}^{\infty} F(z)F(z - \varepsilon\delta)\, dz. \quad (55)$$

The integrand is zero between $z = \pm(\delta + 2/3)$; if $\delta \gg 1$, we can set $F(z) \approx F(\varepsilon\delta)$ and pull it out of the integral. This leads to $\Gamma_2 \approx A\Gamma_0/\delta^4 + B\Gamma_1/\delta^3$ and an inertial mass $\mu_i \approx 42\mu_\oplus\delta^4/(1 + 0.5\delta)$. On the other hand, the distance to nonlinearity is strongly dependent on the secondary's mass, $\delta_{NL} \sim (r^2D'c^6/\pi^2)\Psi^{-4}$, where $D' \equiv rdD/dr$ (e.g., Ward 1986). Again setting $mc/r\Omega \sim 1$, we can write $\mu \approx 0.5h'^2(h'/\delta_{NL})^{1/4}$. Solving these equation yields $\delta_{NL} \sim 2h$, $\mu_i \sim 2 \times 10^{-3} \approx 2\mu_{\rm Jupiter}$, implying that the nonlinear shocks will not stall type I drift until the secondary is of giant planet size. However, as mentioned above, nonlinear effects develop in the launch zone at somewhat lower masses $\mu \gtrsim (h/r)^3 \sim 10^2\mu_\oplus$, due to resonance overlap.

In general, both increasing the damping length and the exponential power pushes the threshold mass up, expanding the domain of type I motion. These important issues will be pursued further in subsequent work.

c. Future Work

Although the calculations presented here constitute an improvement over earlier versions, several relevant features are still omitted or treated inadequately. For the interested reader, these are enumerated in some detail below. Others may wish to skip directly to the Summary.

(i) One shortcoming is the 2D nature of the torque model. However, the fact that Lindblad resonances are prevented from lying closer than $\sim\pm 2h/3$ from the perturber should help mitigate the error introduced by the thin disk torque expressions. Calculations could be improved by using a more generalized and vertically averaged form of Ψ (e.g., Ward 1986, Artymowicz, 1993a).

(ii) The smoothed torque density $T_m|dm/dr|$ should be replaced by the true torque density that is constructed from a superposition of the torque density for each individual wave, $dT/dr \equiv \sum (dT/dr)_m$ (e.g., Takeuchi *et al.* 1996). Each wave must propagate a distance $\lambda_{\rm driving}$ before achieving full amplitude and therefore the perturber must exert its torque over this spatial scale. This will tend to spread out the form factor, making the feedback torque somewhat less sensitive to the damping length of the waves.

(iii) A potentially important issue is the effect of disk tides on the temperature structure of the disk. The disk heats up at rates

$$\left.\frac{dE}{dt}\right|_{\rm tides} = (\Omega_s - \Omega)\frac{dT}{dr}; \qquad \left.\frac{dE}{dt}\right|_{\rm viscous} = 2\pi\sigma\nu r^3\left(\frac{\partial\Omega}{\partial r}\right)^2 \quad (56)$$

due to tides and viscous stresses. The ratio of these two expressions is of order β, so that tidal heating becomes comparable to viscous heating when the mass approaches the viscous mass, μ_ν. Trailing disk material will have been heated longer than leading material, and the resulting differential temperature could weaken the net disk torque by increasing the scale height of the outer material. This may slow the drift rate and help promote transition from type I to type II motion. We show in Appendix D that for the inviscid case, this temperature differential would lead to an additional contribution to the feed back torque, $\Gamma_2 \to \Gamma_2 + \Gamma_{\rm temp}$, where for $F_{\rm ansatz}$, $\Gamma_{\rm temp} \equiv (9/20)(2A/d^3)^2(d + 4/3) = 0.168$. However, the actual effect is likely to be smaller since heating occurs smoothly across the orbit and there are radiation losses.

(iv) Our model should include a contribution from corotation resonances falling at the secondary's orbit (Ward 1993a). Numerical models by Korycansky and Pollack (1993) can be used to estimate the cumulative corotation torque exerted on the secondary,

$$T_c \approx \frac{4}{3}\frac{d\ln(\sigma/B)}{d\ln r}\mu^2\sigma r^2(r\Omega)^2\left(\frac{r\Omega}{c}\right)^2, \quad (57)$$

where $B = \Omega + (r/2)\, d\Omega/dr$ is the vorticity. A crude estimate of its importance can be made by including

$2T_c/Mr_s\Omega_s$ on the RHS of Eq. (18). Its effect on the inviscid solution is immediately obtained by replacing $\Gamma_1 \rightarrow \Gamma_1 + \Gamma_c$, where $\Gamma_c \sim -4h'(3/2 - k)/3\pi = -0.03(3/2 - k)$. Thus, corotation torques could weaken the overall torque asymmetry by ~18% for $k = 0$, but vanish for $k = 3/2$. For still larger k, corotation torques augment the Lindblad torque asymmetry. Indeed, since the libration region is only of width $\sim O(\mu/h')^{1/2}$, it is not the global value of $k(x) \equiv -(r/\sigma)\, d\sigma/dr$, but the local value in the vicinity of $x = 0$ that is pertinent. Inspection of Fig. 15, reveals that the tidal response of the disk tends to generate positive values of k near the protoplanet. Furthermore, this torque weakens due to the libration of disk material, which works to remove the "vortensity" gradient, $d(\sigma/B)/dr$ (Quinn and Goodman 1986, Ward, 1993a).

(v) Another source of disk torque at the protoplanet's orbit is that of gravitationally enhanced drag (e.g., Takeda *et al.* 1985, Ohtsuki *et al.* 1988). The pressure support of the disk [Eq. (10)] results in a differential orbital velocity between disk and protoplanet and a resultant "headwind." It is well-known that this gives rise to a drag on small particles that induces orbital decay. If the so-called gravitational radius, $R_G \equiv GM/c^2$, of a body becomes larger than its physical radius, R, it begins to deflect the flow of gas at that distance, increasing its effective drag cross section to $O(\pi R_G^2)$. This occurs for $R > c/\Omega_*$, where $\Omega_*^2 \equiv \sqrt{4\pi G\rho_P/3} = 5.3 \times 10^{-4}\sqrt{\rho_p}\, s^{-1}$ is the Schuler frequency and ρ_p is the solid density of the object. For a sound speed of, $c \sim$ few $\times 10^5$ cm/s, $R_G \geq O(10^3)$ km, so that mid-stage products of accretion runaway are likely to fall into this size range. Takeda *et al.* have proposed a modification of the drag coefficient for large objects to be used whenever their gravitational radius exceeds their physical radius: $C_D \rightarrow C_D(R_G/R)^2$. This leads to a drift rate of

$$v = c_3\mu(r\Omega)(\sigma r^2/M_p)(r\Omega/c), \tag{58}$$

which is a factor of $O|c_3/c_2|(h/r)^2 \leq 10^{-2}$ slower than Eq. (1). In addition, if the object is large enough to convert to type II drift, gap formation will drive the density down and render such drag effects negligible. Thus the near zone gravitational interaction characterized by enhanced drag is not likely to be competitive with the far zone gravitational interaction described by disk tides (e.g., Ward 1993b).

(vi) Although the shifts in resonance sites have been taken into account in estimating the net undisturbed disk torque, Γ_1, they have not been treated in the disk's tidal response. Resonance shifts become pronounced with the formation of a strong gap such as in Figs. 15d–15f. Pressure gradients on both sides of the gap tend to displace resonance sites further from the protoplanet. An improved model should also treat this effect self-consistently.

(vii) Our use of a single viscosity for both global disk evolution and diffusion near the protoplanet may be an important oversimplification. The presence of the protoplanet may alter the viscous properties of the disk locally. Such an effect is seen for large objects embedded in a particle disk (e.g., Ida and Makino 1993).

(viii) In our brief discussion on nonlocal damping, the dependence of the damping lengths on resonance order was ignored. This makes the damping length an implicit function of the launch point, $\delta(y)$, through Eq. (15) and will cause a further spreading of the disk's form factor.

Finally, since our model is a quasi-steady-state one, it cannot investigate the transitional phase as this state is approached nor estimate the time scales involved. A more comprehensive initial value treatment including many of the above improvements will require numerical modeling. One purpose of this communication is to motivate such an undertaking.

VI. SUMMARY

We have presented a simple analytical model that illustrates two types of protoplanet migration and the transition between them. In the first type of drift, the protoplanet migrates relative to the disk due to torque asymmetries at a rate proportional to its mass and to the surface density of the disk. In the second type of motion, the protoplanet is locked to a circumstellar disk by the formation of a gap. There is negligible motion relative to the disk, and the protoplanet migrates with the disk's viscous evolution and shares its fate. The drift rate is determined by the strength of the viscosity and is independent of the protoplanet mass or the mass of the disk. Cooling the disk increases the type I rate, whereas heating the disk increases the type II rate. Small protoplanets tend to execute type I motion; large protoplanets execute type II. For given values of the viscosity and damping length, there is a critical threshold mass at which type I motion stalls and fairly abruptly converts to type II. However, for reasonable turbulence, type I motion can persist for objects up to the size of giant planet cores even assuming local wave damping. Nonlocal damping of density waves may significantly increase the threshold mass.

The transition (I $\rightarrow$ II) entails a velocity drop of between one and two orders of magnitude. These drift mechanisms can generate considerable mobility and differential motion among protoplanetary objects embedded in a circumstellar gaseous disk. Generally, orbits suffer decay, although type II migration can move outward with the disk in the more remote parts (e.g., Lynden-Bell and Pringle 1974). The orbital lifetime for type I migration is usually much shorter than the lifetime of the nebula. The induced radial drift could assist accretion, but could also destroy the system if newly formed objects decay into the primary.

Finally, we should point out that although opening a gap increases the lifetime of the protoplanet's orbit, decay

into the primary may still eventually occur unless type II migration is also aborted. As suggested by Lin *et al.* (1996), it is an intriguing possibility that the close orbit of the 51 Peg companion (Mayor and Queloz 1995) is a highly evolved state, having decayed from a much larger starting distance. Clearly, these issues place strong constraints on viable conditions for Solar System survival and may help explain the rather low yields in the search for planets around nearby solar-type stars.

APPENDIX A

The torque is given by the downstream angular momentum flux [e.g., Artymowicz, 1993a, Eq. (51)],

$$T_m = -\frac{4\pi\sigma c^2 m}{(1+4\xi^2)\Omega^2} Re\left\{i\frac{dv}{dx}v_*\right\}, \tag{59}$$

where v is the radial perturbation velocity obtained from the equation

$$\left(\frac{d^2}{dx^2} - \frac{Dr^2}{c^2} - m^2\right) v = -\frac{r\Omega}{2c^2}\left(\frac{d}{dx} + 2mf\right)\phi. \tag{60}$$

The effective resonance location, $r_{\rm eff}$, is where

$$D_* \equiv D + m^2c^2/r^2 = 0. \tag{61}$$

Expanding about $r_{\rm eff}$, Eq. (60) can be approximated by

$$\frac{d^2v}{dx^2} - \beta_*(x - x_{\rm eff})v = \frac{r\Omega}{2c^2}\left(\frac{d}{dx} - 2mf\right)\phi|_{\rm eff}. \tag{62}$$

In writing (62), we have evaluated the RHS at $r_{\rm eff}$ and defined $\beta_* = [(r/c)^2 r dD_*/dr]_{\rm eff}$. Equation (62) is a form of Airy's equation. Applying the radiative boundary condition, its solution is (e.g., Ward 1986)

$$v = \frac{\pi}{|\beta_*|^{2/3}}\frac{r\Omega}{2c^2}\left(\frac{d\phi}{dx} + 2mf\phi\right)_{\rm eff}[-\varepsilon i Ai(w) + Gi(w)], \tag{63}$$

where $w \equiv \varepsilon|\beta_*|^{1/3}(x - x_{\rm eff})$ and Ai, Gi are Airy and associated functions. Substituting into Eq. (59) and evaluating the flux as $w \to \infty$ yields

$$T_m = \varepsilon\frac{m\pi^2\sigma(d\phi/dx + 2mf\phi)^2}{(1+4\xi^2)(rdD_*/dr)}. \tag{64}$$

The location of an mth order Lindblad resonance is where

$$\frac{\Omega_{\rm s}}{\Omega} = 1 + \frac{\varepsilon}{m}\left(\frac{\kappa}{\Omega}\right)\sqrt{1+\xi^2}. \tag{65}$$

The derivative of (61), evaluated at resonance, is

$$r\frac{dD_*}{dr} = r\frac{d\kappa^2}{dr} - 2m^2(\Omega - \Omega_{\rm s})r\frac{d\Omega}{dr} + m^2 r\frac{d}{dr}(c/r)^2. \tag{66}$$

Assuming $c^2 \propto T \propto r^{-1}$, this can be rearranged to read

$$\begin{aligned}\frac{dD_*}{dr} = {} & 3\Omega_s m^2(\Omega - \Omega_{\rm s}) + (1-l)\xi^2\kappa^2 + \kappa^2\left(3 + \frac{d\ln\kappa^2}{d\ln r}\right) \\ & - m^2\Omega(\Omega - \Omega_{\rm s})\left(3 + \frac{d\ln\Omega^2}{d\ln r}\right).\end{aligned} \tag{67}$$

For nearly Keplerian disks the last two terms are small and are ignored. Using (61) this can be further simplified to

$$r\frac{dD_*}{dr} = -3\varepsilon m\kappa\Omega_{\rm s}\sqrt{1+\xi^2} + (1-l)\xi^2\kappa^2. \tag{68}$$

Substitution of (6), (9), and (68) into (64) gives

$$T_m = \varepsilon\frac{4}{3}\frac{m^2\mu^2(\sigma r_{\rm s}^2)(r_{\rm s}\Omega_{\rm s})^2\hat{\psi}^2}{(1+4\xi^2)\sqrt{1+\xi^2}}\left(\frac{\Omega_{\rm s}}{\kappa}\right)\left[1 - \frac{\varepsilon(1-l)\xi^2\kappa}{3\sqrt{1+\xi^2}m\Omega_{\rm s}}\right]^{-1}, \tag{69}$$

where $\xi^2 = \xi_{\rm s}^2/\alpha_r^{l-1}$. Setting $\kappa \approx \Omega$ yields Eq. (8) in the text. To compute $\alpha_{\rm r}$, we use Eq. (10). To lowest order, the resonance condition becomes

$$\frac{\Omega_{\rm s}}{\Omega_{\rm K}} = 1 + \frac{\varepsilon}{m}\sqrt{1+\xi^2} - \frac{1}{2}(k+l)\frac{c^2}{(r\Omega_{\rm K})^2} = \alpha_r^{3/2}. \tag{70}$$

This should be solved by iteration with $\xi(m, \alpha_r)$.

APPENDIX B

To expose the asymmetries in ψ, it is useful to approximate the Laplace coefficients in terms of modified Bessel functions (GT80),

$$b_{1/2}^m(\alpha_r) \approx \frac{2}{\pi}\frac{K_0(\Lambda)}{\sqrt{\alpha_r}}; \qquad \Lambda \equiv \frac{m|\alpha_r - 1|}{\sqrt{\alpha_r}}. \tag{71}$$

(Note that this is a slightly more accurate expression than used in earlier works, viz., GT80.) Differentiation of (71) yields

$$\alpha_r\frac{d}{d\alpha_r}b_{1/2}^m = -\frac{2}{\pi}\left[\frac{\varepsilon m}{2}\left(1 + \frac{1}{\alpha_r}\right)K_1 + \frac{K_0}{2\sqrt{\alpha_r}}\right], \tag{72}$$

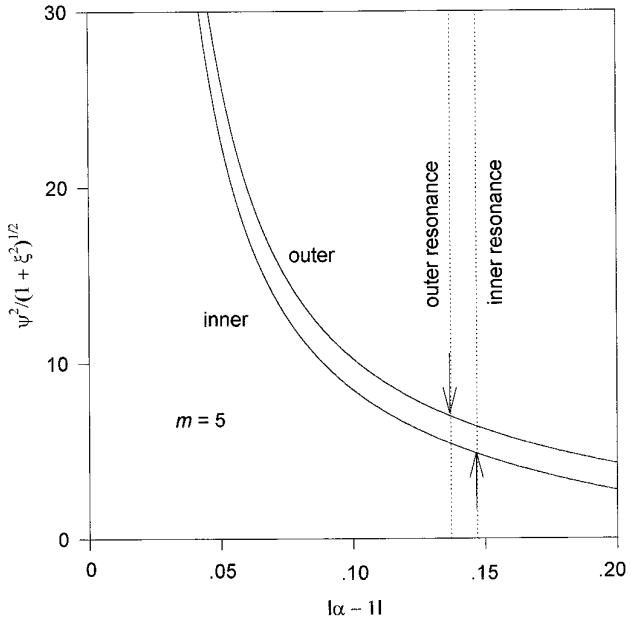

FIG. 18. Asymmetries associated with the resonant perturbations of the disk. The forcing amplitude, ψ, is systematically larger for the outer portion of the disk. In addition, outer resonances lie slightly closer than inner ones, sampling the disturbing potential at a larger value.

and substitution into Eq. (9) yields

$$\psi = \frac{1}{2}\left(1 + \frac{1}{\alpha_r}\right) K_1(\Lambda) + \left(2m|\alpha_r^{3/2} - 1| + \frac{\varepsilon}{2m}\right)\frac{K_0(\Lambda)}{\sqrt{\alpha_r}}. \tag{73}$$

The behavior of $\psi^2/\sqrt{1+\xi^2}$ for $m = 5$ is shown in Fig. 18 as a function of $|\alpha_r - 1|$ both inside and outside the orbit. The outside forcing function is stronger in the vicinity of resonance.

Now consider a Keplerian disk for which Eq. (70) reduces to

$$\alpha_r - 1 = \left(1 + \frac{\varepsilon}{m}\sqrt{1+\xi^2}\right)^{2/3} - 1 \approx \frac{2\varepsilon}{3m}\sqrt{1+\xi^2} - \frac{1+\xi^2}{9m^2}. \tag{74}$$

Outer resonances lie closer to the perturber and sample a larger value of the forcing function (Fig. 18). In particular, the argument of the Bessel functions reads

$$\Lambda \approx \frac{2}{3}\sqrt{1+\xi^2} - \frac{\varepsilon}{3}\frac{1+\xi^2}{m}. \tag{75}$$

Expanding ψ yields,

$$\begin{aligned}\psi \approx [K_1 + 2\sqrt{1+\xi^2}K_0] + \frac{\varepsilon}{m}\Bigg[\left(\frac{1}{6} - \frac{\xi^2}{3}\right)K_0 \\ + \left(\frac{5}{6} + \frac{2\xi^2}{3}\right)\sqrt{1+\xi^2}K_1\Bigg] = \psi_0 + \varepsilon\,\Delta\psi.\end{aligned} \tag{76}$$

Here the Bessel functions are to be evaluated at $\Lambda_0 \equiv (2/3)\sqrt{1+\xi^2}$. Squaring this and multiplying by $\alpha_r^{3/2} = 1 + (\varepsilon/m)\sqrt{1+\xi^2}$ leads to $\alpha_r^{3/2}\psi^2 \approx \psi_0^2 + \psi_0[2\,\Delta\psi + (\varepsilon/m)\sqrt{1+\xi^2}\psi_0]$, where the bracketed quantity is

$$\begin{aligned}2\,\Delta\psi + \frac{\varepsilon}{m}\sqrt{1+\xi^2}\psi_0 \approx \frac{\varepsilon}{m}\Bigg[\left(2\sqrt{1+\xi^2} + \frac{1}{3} - \frac{2\xi^2}{3}\right)K_0 \\ + \left(\sqrt{1+\xi^2} + \frac{5}{3} + \frac{4\xi^2}{3}\right)\sqrt{1+\xi^2}K_1\Bigg].\end{aligned} \tag{77}$$

The limit $\xi \to 0$, recovers Ward's (1986) value, $(\varepsilon/3m)(7K_0(2/3) + 8K_1(2/3))$.

The fractional difference between inner and outer values of ψ^2 is $\sim 4|\Delta\psi|/\psi_0$, while the fractional difference in κ is $\sim(2/m)\sqrt{1+\xi^2}$. For $\xi \ll 1$, these values read $\sim(2/3m)[5K_1(2/3) + K_0(2/3)]/[K_1(2/3) + 2K_0(2/3)] \sim 1.67/m$ and $2/m$, respectively.

APPENDIX C

To chose an *ansatz* form, we first need to reproduce the correct behavior at $x \gg 1$, $\xi \ll 1$, for which $F(x) \propto \varepsilon m^4 \alpha_r^2 \psi^2$. The m^4 dependence yields the usual lowest order term, $\varepsilon A/x^4$, for the torque density. The asymmetry comes mostly from $\alpha_r^2\psi^2$, which has an explicit dependence on ε/m, as well as an implicit one through $\Lambda \to 2/3(1 - \varepsilon/3m)$. Expanding to first order in $1/m$, leads to an additional term of the form, $B/|x^3|$. Next, at the other limit, $\xi \gg 1$, $F(x) \propto \varepsilon m^2 \alpha_r^2 \psi^2$ with $\Lambda \to 2\xi/3$. The asymptotic form of the Bessel functions, $K_i(\Lambda) \approx e^{-\Lambda}\sqrt{\pi/2\Lambda}$, kills the torque at large $\xi \sim 1/\sqrt{(3x/2)^2 - 1}$, i.e., as $x \to \pm 2/3$. This suggests that the steep cutoff could be mimicked by multiplying each term of the ansatz by a killing factor of form, $e^{-|d/z|}$, where $z \equiv x - 2\varepsilon/3$. Equation (46) satisfies these requirements and is integrable.

We use the summation values to set

$$\frac{A}{d^3} = \frac{1}{4}\sum|\hat{T}_m| = 0.198; \qquad \frac{B}{d^2} = \frac{1}{2}\sum\hat{T}_m = 0.124. \tag{78}$$

Squaring Eq. (46) yields

$$F^2(x) = \left[\frac{A^2}{z^8} + 2\frac{AB}{z^7} + \frac{B^2}{z^6}\right]e^{-2|d/z|}. \tag{79}$$

By symmetry, integration of the second term vanishes, leaving

$$\int_{-\infty}^{\infty} F^2(x)\,dx = 2A^2\int_0^{\infty} e^{-2(d/z)}\frac{dz}{z^8} + 2B^2\int_0^{\infty} e^{-2(d/z)}\frac{dz}{z^6}. \tag{80}$$

Using the identity

$$\int_0^{\infty} e^{-2(d/x)^n}\frac{dx}{x^m} = \frac{1}{nd^{m-1}2^{(m-1)/n}}\int_0^{\infty} e^{-t}t^{(m-1)/n}\frac{dt}{t} = \frac{\Gamma((m-1)/n)}{nd^{m-1}2^{(m-1)/n}}, \tag{81}$$

we can write,

$$\int_{-\infty}^{\infty} F^2(x)\,dx = \frac{1}{d}\left(\frac{\Gamma(7)}{2^6}\left(\frac{A}{d^3}\right)^2 + \frac{\Gamma(5)}{2^4}\left(\frac{B}{d^2}\right)^2\right) = \Gamma_2 = 0.443, \tag{82}$$

where here, $\Gamma(t)$, denotes the gamma function of t. From Eqs. (78) and (82) we find, $A = 0.228$, $B = 0.136$, and $d = 1.05$.

APPENDIX D

A rough assessment of this effect can be made by ignoring any additional radiation by the disk, and assuming all tidal heating goes to increase the disk temperature, $2\pi r\sigma C_p DT/Dt = dE/dt|_{\text{tides}}$, where C_p is the specific

heat in ergs/g-K. The temperature of the disk is found from the equation of energy balance

$$2\pi r\sigma C_p \frac{DT}{Dt} = 2\pi\sigma\nu r^3 \left(\frac{\partial\Omega}{\partial r}\right)^2 + (\Omega_s - \Omega)\frac{dT}{dr} - 2\pi r\sigma_{SB}\tilde{\varepsilon}T^4, \quad (83)$$

where σ_{SB} is the Stefan–Boltzman constant and $\tilde{\varepsilon}$ is the emissivity. Let $T_o(x)$ be the solution in the absence of tidal heating, and $\Delta T \equiv T - T_o$. Assuming that the temperature increment can also be expressed as kinematic wave, $D\,\Delta T/Dt \rightarrow (v - v_s)\partial\Delta T/\partial r$,

$$\frac{1}{h'}\frac{d}{dx}\left(\frac{\Delta T}{T}\right) + \frac{r\tilde{\varepsilon}\sigma_{SB}(T^4 - T_o^4)}{\sigma C_p(v - v_s)} \approx \frac{1}{2}\left(\frac{\mu}{h_s'^2}\right)^2 \left(\frac{r_s^2\Omega_s^2}{C_pT}\right)\frac{r(\Omega_s - \Omega)F}{(v - v_s)}. \quad (84)$$

For a diatomic gas, $C_pT = 5c^2/2$. An upper bound on the heating is given by ignoring the second term on the LHS, which gives the additional radiation loses due to the higher temperature. This leads to a temperature increment,

$$\frac{\Delta T(x)}{T} \approx \frac{3}{10}\left(\frac{\mu}{h'^2}\right)^2 \int_{-\infty}^{x} \frac{yF(y)}{(\hat{v} - \hat{v}_s)}\,dy, \quad (85)$$

where the specific heat ratio for an ideal diatomic gas is used. As a rough estimate, assume the temperature of the outer disk exceeds the inner by $\Delta T(\infty)$. Defining[10] $H \equiv h/h_s$ and keeping only the symmetric part of the torque density, the form factor reads $F(x, H) \sim H^{-4}F(x/H)$. The integration $\int_0^\infty F(x, H)\,dx = H^{-3}\int_0^\infty F(x/H)d(x/H) \sim 2(A/d^3)(1 \pm 3\,\Delta h/h + \cdots)$, where the $+(-)$ refers to the inner (outer) disk. Since $h \propto \sqrt{T}$, $\Delta h/h = (1/2)\,\Delta T/T$. Integrating Eq. (85) yields $\int_{-\infty}^{\infty} xF(x)\,dx = (2A/d^3)(d + 4/3)$, where we have assumed $\hat{v}_s \gg \hat{v}$ and pulled the secondary's velocity out of the integral.

ACKNOWLEDGMENTS

The research described in this paper was carried out at the Jet Propulsion Laboratory, California Institute of Technology under contract with the National Aeronautics and Space Administration. The author thanks an anonymous referee for several valuable comments that greatly improved the quality of this work. The author also thanks the San Juan Capistrano Research Institute for their hospitality during a portion of this project.

REFERENCES

Araki, S., and W. R. Ward 1995. Shepherding in a disk of low optical depth. *Bull. Am. Astron. Soc.* **23,** 169.

Artymowicz, P. 1993a. On the wave excitation and a generalized torque formula for Lindblad resonances excited by external potential. *Astrophys. J.* **419,** 155–165.

Artymowicz, P. 1993b. Disk–satellite interaction via density waves and the eccentricity evolution of bodies embedded in disks. *Astrophys. J.* **419,** 166–180.

Artymowicz, P., and S. H. Lubow 1996. Dynamics of binary–disk interaction. Mass flow through gaps. *Astrophys. J. Lett.,* submitted.

Beauge, C., S. J. Aarseth, and S. Ferraz-Mello 1994. Resonance capture and the formation of the outer planets. *Mon. Not. R. Astron. Soc.* **270,** 21–34.

Beckwith, S. V. W., and A. I. Sargent 1993. The occurrence and properties of disks around young stars. In *Protostars and Planets III,* p. 521. Univ. of Arizona Press, Tucson.

Black, D. 1995. Completing the Copernican revolution: The search for other planetary systems. *Annu. Rev. Astron. Astrophys.* **33,** 359–380.

Cabot, W., V. M. Canuto, O. Hubickyj, and J. B. Pollack 1987. The role of turbulent convection in the primitive solar nebula. I. Theory. *Icarus* **69,** 387–422.

Cassen, P., and D. S. Woolum 1996. Radiatively damped density waves in optically thick protostellar disks. *Astrophys. J.,* in press.

Cochran, W. D., and A. P. Hatzes 1993. McDonald Observatory planetary search: A high precision stellar radial velocity survey for other planetary systems. In *Planets Around Pulsars* (J. A. Philips, S. E. Thorsett, and S. R. Kulkarni, Eds.), p. 267.

Dubrulle, B. 1993. Differential rotation as a source of angular momentum transfer in the solar nebula. *Icarus* **106,** 59–76.

Goldreich, P., and S. Tremaine 1978. The formation of the Cassini division in Saturn's rings. *Icarus* **34,** 240–253.

Goldreich, P., and S. Tremaine 1979. The excitation of density waves at the Lindblad and corotation resonances by an external potential. *Astrophys. J.* **233,** 857–871.

Goldreich, P., and S. Tremaine 1980. Disk–satellite interactions. *Astrophys. J.* **241,** 425–441.

Greenberg, R., J. Wacker, W. K. Hartman, and C. R. Chapman 1978. Planetesimals to planets: Numerical simulation of collisional evolution. *Icarus* **35,** 1–26.

Hayashi, C., K. Nakazawa, and I. Adachi 1977. Long-term behavior of planetesimals and the formation of the planets. *Publ. Astron. Soc. Jpn.* **29,** 163–196.

Hourigan, K., and W. R. Ward 1984. Radial migration of preplanetary material: Implications for the accretion time scale problem. *Icarus* **60,** 29–39.

Korycansky, D. G., and J. B. Pollack 1993. Numerical calculations of the linear response of a gaseous disk to a protoplanet. *Icarus* **102,** 105–165.

Ida, S., and J. Makino 1993. Scattering of planetesimals by a protoplanet: Slowing down of runaway growth. *Icarus* **106,** 210–227.

Levin, B. J. 1978. Relative velocities of plentesimals and the early accumulation of planets. *Moon Planets* **19,** 289–296.

Lin, D. N. C., P. Bodenheimer, and D. C. Richardson 1996. Orbital migration of the planetary companion of 51 Pages to its present location. *Nature* **380,** 606–607.

Lin, D. N. C., and J. Papaloizou 1986a. On the tidal interaction between protoplanets and the primordial solar nebula II. Self-consistent nonlinear interaction. *Astrophys. J.* **307,** 395–409.

Lin, D. N. C., and J. Papaloizou 1986b. On the tidal interaction between protoplanets and the primordial solar nebula. III. Orbital migration of protoplanets. *Astrophys. J.* **309,** 846–857.

Lin, D. N. C., and J. Papaloizou 1993. On the tidal interaction between protostellar disks and companions. In *Protostars and Planets III* (E. H. Levy and J. I. Lunine, Eds.), pp. 749–836. Univ. of Arizona Press, Tucson.

Lin, D. N. C., J. Papaloizou, and G. Savonije 1990. Wave propagation in gaseous accretion disks. *Astrophys. J.* **364,** 326–334.

Lissauer, J. J. 1993. Planet Formation. *Annu. Rev. Astron. Astrophys.* **31,** 129–174.

Lissauer, J. J., and J. N. Cuzzi 1985. Rings and moons: Clues to under-

[10] Not to be confused with the specific angular momentum of Section III.

standing the solar nebula. In *Protostars and Planets II,* pp. 920–956. Univ. of Arizona Press, Tucson.

LISSAUER, J. J., AND G. R. STEWART 1993. Growth of planets from planetesimals. In *Protostars and Planets III,* pp. 1061–1088. Univ. of Arizona Press, Tucson.

LYNDEN-BELL, D., AND A. J. KALNAJS 1972. On the generating mechanism of spiral structure. *Mon. Not. R. Astron. Soc.* **157,** 1–30.

LYNDEN-BELL, D., AND J. E. PRINGLE 1974. The evolution of viscous disks and the origin of the nebula variables. *Mon. Not. R. Astron. Soc.* **168,** 603–637.

MAYOR, M., AND D. QUELOZ 1995. A Jupiter-mass companion to a solar-type star. *Nature* **378,** 355–359.

MARCY, G. W., AND R. P. BUTLER 1992. Precision radial velocities using an iodine absorption cell. In *Seeking Other Planetary Systems: The Role of Stellar Radial Velocity Measurements* (D. W. Latham, Ed.), p. 66. Harvard–Smithsonian Center for Astrophysics.

MCMILLAN, R. S., T. L. MOORE, M. L. PERRY, AND P. H. SMITH 1994. Long, accurate time series measurements of radial velocities of stars. *Astrophys. Space Sci.* **212,** 271–280.

MEYER-VERNET, N., AND B. SICARDY 1987. On the physics of resonant disk-satellite interaction. *Icarus* **69,** 157–175.

OHTSUKI, K., Y. NAKAGAWA, AND K. NAKAZAWA 1988. Growth of the Earth in nebula gas. *Icarus* **75,** 552–565.

PAPALOIZOU, J., AND D. N. C. LIN 1984. On the tidal interaction between protoplanets and the primordial solar nebula. I. Linear calculation of the role of angular momentum exchange. *Astrophys. J.* **285,** 818–834.

PODOLAK, M., W. B. HUBBARD, AND J. B. POLLACK 1993. Gaseous accretion and the formation of the giant planets. In *Protostars and Planets III* (E. H. Levy and J. I. Lunine, Eds.), pp. 1109–1148. Univ. of Arizona Press, Tucson.

QUINN, P. J., AND J. GOODMAN 1986. Sinking satellites of spiral systems. *Astrophys. J.* **309,** 472–495.

RUDEN, S. P., AND D. N. C. LIN 1986. The global evolution of the primordial solar nebula. *Astrophys. J.* **308,** 883–901.

RUDEN, S. P., AND J. B. POLLACK 1991. The dynamical evolution of the protosolar nebula. *Astrophys. J.* **375,** 740–760.

SHU, F. H. 1984. Waves in planetary rings. In *Planetary Rings,* pp. 513–561. Univ. of Arizona Press, Tucson.

SHU, F. H., J. N. CUZZI, AND J. J. LISSAUER 1983. Bending waves in Saturn's rings. *Icarus* **53,** 185–206.

SHU, F. H., D. JOHNSTONE, AND D. HOLLENBACH 1993. Photoevaporation of the solar nebula and the formation of the giant planets. *Icarus* **106,** 92–101.

TAKEDA, H., T. MATSUDA, K. SAWADA, AND C. HAYASHI 1985. Drag on a gravitating sphere moving through gas. *Prog. Theor. Phys.* **74,** 272–287.

TAKEUCHI, T., S. M. MIYAMA, AND D. N. C. LIN 1996. Gap formation in protoplanetary disks. *Astrophys. J.,* **460,** 832.

TREMAINE, S., AND M. D. WEINBERG 1984. Dynamical friction in spherical systems. *Mon. Not. R. Astron. Soc.* **209,** 727–757.

WALKER, G. A. H., A. R. WALKER, A. W. IRWIN, A. M. LARSON, S. L. S. YANG, AND D. C. RICHARDSON 1995. A search for Jupiter-mass companions to nearby stars. *Icarus* **116,** 359–375.

WALTER, F. M. 1986. X-ray sources in regions of star formation. I. The naked T tauri stars. *Astrophys. J.* **306,** 573–586.

WALTER, F. M., A. BROWN, R. D. MATHIEU, P. C. MEYERS, AND F. J. VRBA 1988. X-ray sources in regions of star formation. III. Naked T tauri stars associated with the Taurus–Auriga complex. *Astron. J.* **96,** 297–325.

WARD, W. R. 1982. Tidal barriers in the solar nebula. *Lunar and Planetary Abstracts XIII,* 831–832.

WARD, W. R. 1985. *Density waves in satellite precursor discs.* Proceedings of the Solid Bodies of the Outer Solar System Conference, Vulcano, Italy, September 1985.

WARD, W. R. 1986. Density waves in the solar nebula: Differential Lindblad torque. *Icarus* **67,** 164–180.

WARD, W. R. 1988. On disk–planet interaction and orbital eccentricities. *Icarus* **73,** 330–348.

WARD, W. R. 1989. On the rapid formation of giant planet cores. *Astrophys. J. Lett.* **345,** L99–L102.

WARD, W. R. 1993a. Density waves in the solar nebula: Planetesimal velocities. *Icarus* **106,** 274–287.

WARD, W. R. 1993b. Disk–planet interactions: Torques from the coorbital zone. *Anal. NY Acad. Sci.* **675,** 314–323.

WARD, W. R. 1996. Planetary accretion. In *Proceedings of ASP Symposium on Completing the Inventory of the Solar System.* (T. W. Rettig and J. M. Hahn, Eds.), ASP Conference Series, pp. 337–361.

WARD, W. R., AND J. M. HAHN 1995. Disk tides and accretion runaway. *Astrophys. J. Lett.* **440,** L25–L28.

WARD, W. R., AND K. HOURIGAN 1989. Orbital migration of protoplanets: The initial limit. *Astrophys. J.* **347,** 490–495.

WEIDENSCHILLING, S. J. 1977. Aerodynamics of solid bodies in the solar nebula. *Mon. Not. R. Astron. Soc.* **180,** 57–70.

WETHERILL, G. W. 1990. Formation of the earth. *Annu. Rev. Earth Planet Sci.* **18,** 205–256.

WETHERILL, G. W., AND G. R. STEWART 1989. Accumulation of a swarm of small planetesimals. *Icarus* **77,** 330–357.

WOLSZCZAN, A. 1994. Confirmation of Earth-mass planets orbiting the millisecond pulsar PSR B1257+12. *Science* **264,** 538–542.